



# Targeting PARP11 to avert immunosuppression and improve CAR T therapy in solid tumors

Hongru Zhang<sup>1</sup>, Pengfei Yu<sup>1</sup> , Vivek S. Tomar<sup>1</sup>, Xiangjie Chen<sup>2</sup>, Matthew J. Atherton<sup>1,3</sup>, Zhen Lu<sup>1</sup>, Hong-Guang Zhang<sup>2</sup>, Shifeng Li<sup>4</sup>, Angelica Ortiz<sup>1</sup>, Jun Gui<sup>1</sup>, N. Adrian Leu<sup>1</sup>, Fangxue Yan<sup>1</sup>, Andres Blanco<sup>1</sup>, Mirella L. Meyer-Ficca<sup>1</sup> , Ralph G. Meyer<sup>5</sup>, Daniel P. Beiting<sup>6</sup>, Jinyang Li<sup>7</sup>, Selene Nunez-Cruz<sup>7</sup>, Roddy S. O'Connor<sup>7</sup>, Lexus R. Johnson<sup>8</sup>, Andy J. Minn<sup>8,9</sup>, Subin S. George<sup>10</sup>, Constantinos Koumenis<sup>8</sup>, J. Alan Diehl<sup>11</sup>, Michael C. Milone<sup>1</sup> , Hui Zheng<sup>1</sup> and Serge Y. Fuchs<sup>1</sup>

**Evasion of antitumor immunity and resistance to therapies in solid tumors are aided by an immunosuppressive tumor microenvironment (TME). We found that TME factors, such as regulatory T cells and adenosine, downregulated type I interferon receptor IFNAR1 on CD8<sup>+</sup> cytotoxic T lymphocytes (CTLs). These events relied upon poly-ADP ribose polymerase-11 (PARP11), which was induced in intratumoral CTLs and acted as a key regulator of the immunosuppressive TME. Ablation of PARP11 prevented loss of IFNAR1, increased CTL tumorcidal activity and inhibited tumor growth in an IFNAR1-dependent manner. Accordingly, genetic or pharmacologic inactivation of PARP11 augmented the therapeutic benefits of chimeric antigen receptor T cells. Chimeric antigen receptor CTLs engineered to inactivate PARP11 demonstrated a superior efficacy against solid tumors. These findings highlight the role of PARP11 in the immunosuppressive TME and provide a proof of principle for targeting this pathway to optimize immune therapies.**

In addition to relative paucity of specific tumor-derived antigens<sup>1–3</sup>, the evasive strategies utilized in the TME by solid tumors are central to their ability to escape from immune surveillance and to resist immune therapies<sup>4,5</sup>. Although new therapeutic approaches have emerged to target diverse cellular or acellular TME components such as regulatory T ( $T_{reg}$ ) or myeloid suppressive cells<sup>6,7</sup> or immunosuppressive cytokines and adenosine<sup>8,9</sup>, the sheer redundancy of these factors hinders the progress of anticancer therapies<sup>2,4,5,10</sup>. Clinical success of immune-checkpoint inhibitors<sup>11</sup> highlights the benefits of approaches that involve identification and targeting of critical unifying mechanisms commonly deployed by diverse immunosuppressive elements to inactivate native or chimeric antigen receptor (CAR)-bearing CTLs.

One facet of immune suppression encountered by CTLs in the TME is linked to their deprivation of type I interferons (IFN1)<sup>12</sup>. In the TME, IFN1 produced by malignant and benign cells elicits numerous paracrine and autocrine effects that significantly contribute to regulation of many aspects of immune surveillance (reviewed elsewhere<sup>13,14</sup>). Moreover, responses to many types of anticancer treatments, including chemotherapy and radiotherapy, depend on the functional IFN1 pathway. Expression of interferon (IFN)-stimulated genes in malignant cells may be associated with diminished antitumor immune responses and resistance to immune

therapies<sup>15</sup>; however, activities of CTLs often rely on IFN1, which normally provides a ‘third signal’ to support clonal expansion of CD8<sup>+</sup> T cells<sup>16–18</sup> and maintains the viability of these cells upon their activation<sup>19</sup>.

However, in intratumoral cells, the IFN1 pathway is inactivated because of downregulation of the IFNAR1 receptor chain, which is required for all cellular responses to IFN1 (refs. <sup>12,13</sup>). The TME stress and tumor-derived factors accelerate downregulation of IFNAR1 (refs. <sup>20–23</sup>) by stimulating its phosphorylation and recruitment of the  $\beta$ -TrCP-containing E3 ubiquitin ligase, which facilitates IFNAR1 ubiquitination, endocytosis and degradation (reviewed previously<sup>12</sup>). The levels of  $\beta$ -TrCP can be regulated by Wnt pathway-driven messenger RNA stabilization<sup>24</sup> or protein stabilization dependent on the mono-ADP-ribosylation activity of PARP11 (ref. <sup>25</sup>), but the mechanisms by which these processes are modulated in the TME and, specifically, in intratumoral CTLs remain poorly understood.

Deprived from the prosurvival effects of IFN1, activated intratumoral CTLs rapidly die, thereby vacating the immune-privileged niches inside the tumor<sup>19</sup>. Accordingly, CTLs and CAR T cells deficient in p38 $\alpha$  kinase, which is critical for IFNAR1 phosphorylation and  $\beta$ -TrCP recruitment<sup>26</sup>, or engineered to express a stabilized IFNAR1<sup>S526A</sup> receptor mutant (SA<sup>21</sup>), survive better inside solid

<sup>1</sup>Department of Biomedical Sciences, School of Veterinary Medicine, University of Pennsylvania, Philadelphia, PA, USA. <sup>2</sup>Institutes of Biology and Medical Sciences and Jiangsu Key Laboratory of Infection and Immunity, Soochow University, Suzhou, China. <sup>3</sup>Department of Clinical Sciences & Advanced Medicine, School of Veterinary Medicine, University of Pennsylvania, Philadelphia, PA, USA. <sup>4</sup>Dept. of Intensive Care Medicine, First Affiliated Hospital of Soochow University, Suzhou, China. <sup>5</sup>Department of Animal, Dairy, and Veterinary Sciences, College of Agriculture and Applied Sciences and School of Veterinary Medicine, Utah State University, Logan, UT, USA. <sup>6</sup>Department of Pathobiology, School of Veterinary Medicine, University of Pennsylvania, Philadelphia, PA, USA. <sup>7</sup>Department of Pathology and Laboratory Medicine, Perelman School of Medicine, University of Pennsylvania, Philadelphia, PA, USA. <sup>8</sup>Department of Radiation Oncology, Perelman School of Medicine, University of Pennsylvania, Philadelphia, PA, USA. <sup>9</sup>Mark Foundation Center for Immunotherapy, Immune Signaling, and Radiation, University of Pennsylvania, Philadelphia, PA, USA. <sup>10</sup>Institute for Biomedical Informatics, Perelman School of Medicine, University of Pennsylvania, Philadelphia, PA, USA. <sup>11</sup>Department of Biochemistry, Case Comprehensive Cancer Center, Case Western Reserve University, Cleveland, OH, USA. e-mail: syfuchs@upenn.edu

tumors. Inexplicably, these SA or p38-deficient CTLs remain active against tumors despite the presence of immunosuppressive TME elements<sup>19,27</sup>. Understanding the mechanisms underlying this paradox is important for designing approaches to reactivate the IFN1 pathway and to increase the viability and activity of the intratumoral CTL.

Our present study demonstrates that downregulation of IFNAR1 on tumor CTLs is driven by T<sub>reg</sub> cells and adenosine. This downregulation of IFNAR1 is required for suppression of the tumoricidal activities of CTLs. PARP11, which is induced in the intratumoral CTLs, plays a major role in IFNAR1 downregulation and inactivation of CTLs. Accordingly, CAR T cells engineered to downregulate PARP11 or combined with a pharmacologic inhibitor display an increased antitumor activity *in vivo*.

## Results

**Downregulation of IFNAR1 on CTL undermines their activities.** We posited that IFNAR1 inactivation enables the cellular and acellular elements of the TME to suppress the tumoricidal activities of CTLs. To test this hypothesis, we interrogated gene expression in the intratumoral wild-type (WT) or SA CTLs at a single-cell level. CTLs isolated from tumors growing in knock-in SA mice (Extended Data Fig. 1a) indeed expressed greater levels of IFNAR1 (Fig. 1a) and when profiled for gene expression (Fig. 1b and Extended Data Fig. 1b), exhibited increased IFN signatures (Fig. 1c,d) compared to WT intratumoral CTLs. Furthermore, downregulation of IFNAR1 in WT CTLs was associated with diminished polyfunctional memory and effector signatures (Fig. 1d), increased expression of exhaustion-related genes (Fig. 1e) and decreased cytotoxic and activated CTL gene expression patterns (Fig. 1f,g and Extended Data Fig. 1c).

Accordingly, intratumoral WT CTLs displayed a decrease in the activation/cytotoxic markers such as IFN- $\gamma$ , Granzyme B/FasL and CD69 compared to SA CTLs (Fig. 1h and Extended Data Fig. 1d,e). These data suggest that inactivation of intratumoral CTLs is associated with IFNAR1 downregulation in the TME. Plausibly, this downregulation may stimulate immunosuppressive elements (as reported for granulocytic myeloid-derived suppressor cells<sup>28</sup>) or render active CTLs sensitive to these elements, or both.

To focus on the roles of IFNAR1 downregulation on CTLs, we analyzed functional tumoricidal activities of CTLs using an *in vitro* assay where OT-1 CTLs (WT or SA) killed OVA-expressing MC38 tumor cells. As a representative component of the immunosuppressive TME, we used T<sub>reg</sub> cells. Downregulation of IFNAR1 and inhibition of cytolytic activity were observed upon co-incubation of WT OT-1 CTLs with T<sub>reg</sub> cells, which were either *in vitro* differentiated (iT<sub>reg</sub> cells; Fig. 2a,b and Extended Data Fig. 2a) or isolated from WT tumors (Extended Data Fig. 2b). Of note, SA OT-1 CTLs maintained their IFNAR1 surface levels and, remarkably, were

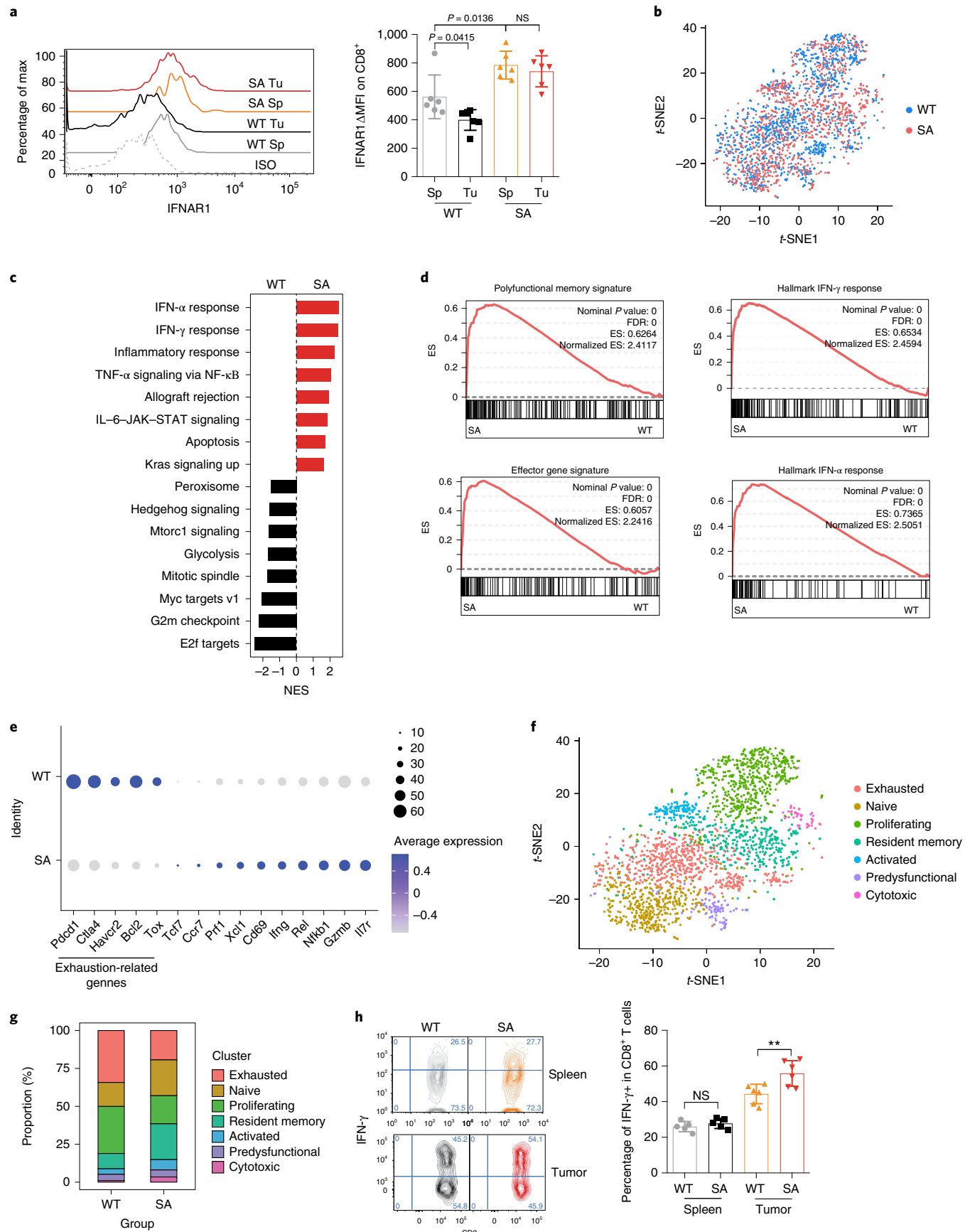
insensitive to inhibition of tumoricidal activity by T<sub>reg</sub> cells (Fig. 2a,b and Extended Data Fig. 2a,b) indicating that IFNAR1 downregulation on CTLs contributes to the suppressive activity of T<sub>reg</sub> cells.

**Adenosine downregulates IFNAR1 on CTL.** T<sub>reg</sub> cells deploy diverse suppressive mechanisms involving production of adenosine, prostaglandins and cytokines such as transforming growth factor (TGF)- $\beta$  (reviewed previously<sup>6,29</sup>). Inhibitors of adenosine production and signaling have been extensively studied as the means to reactivate antitumor immunity<sup>8,9</sup>. An inhibitor of adenosine receptor A2AR, CPI-444, limited suppressive effects of T<sub>reg</sub> cells on IFNAR1 levels and cytotoxic activities (Fig. 2c,d). Consistently, adding adenosine to WT OT-1 CTLs notably downregulated IFNAR1 (Fig. 2e and Extended Data Fig. 2c) and IFN-stimulated genes (Fig. 2f). Furthermore, adenosine also inhibited WT CTL activity as manifested by decreased IFN- $\gamma$  expression (Fig. 2g) and attenuated tumoricidal effects (Fig. 2h and Extended Data Fig. 2). Notably, adenosine decreased neither IFNAR1 levels nor cytotoxicity in the SA CTL (Fig. 2e-h and Extended Data Fig. 2c,d) suggesting that downregulation of IFNAR1 on CTLs triggered by cellular (T<sub>reg</sub>) and acellular (adenosine) elements of the TME plays a key role in CTL inactivation.

We next sought to determine whether IFNAR1 in CTLs is required for their antitumor function and whether reactivation of CTLs by A2AR inhibitor CPI-444 was dependent on ability of this agent to prevent downregulation of IFNAR1. These assumptions were indeed supported by *in vivo* studies, in which genetic ablation of IFNAR1 in CD8 $^{+}$  T cells (Extended Data Fig. 2e-g) accelerated tumor growth and notably abrogated the therapeutic effects of CPI-444 (Fig. 2i,j). Collectively these data suggest that downregulation of IFNAR1 on CTLs renders them prone to the immunosuppressive elements of the TME. In addition, these findings indicate that stabilization of IFNAR1 in CTLs plays an important role for therapeutic efficacy of the adenosine receptor inhibitor and provides the rationale for stabilizing IFNAR1 for reactivation of the intratumoral CTL.

**PARP11 acts as a key regulator of the immunosuppressive TME.** Degradation of phosphorylated IFNAR1 depends on activity of the Skp1-Cullin1-Rbx1 E3 ubiquitin ligase recruited by the  $\beta$ -TrCP F-box proteins, including  $\beta$ -TrCP1 encoded by the *BTRC* gene or  $\beta$ -TrCP2/HOS encoded by the *FBXW11* gene<sup>30-32</sup>. These  $\beta$ -TrCP proteins themselves are the substrates for the core ligase<sup>33</sup> and stability and availability of  $\beta$ -TrCP to ubiquitinate phosphorylated IFNAR1 is regulated by mono-ADP ribosyltransferase PARP11 (ref. 25). Treatment of T cells with adenosine stimulated phosphorylation, ubiquitination and downregulation of IFNAR1 (Fig. 3a). An adenosine-triggered decrease in IFNAR1 levels coincided with activation of p38 $\alpha$ , upregulation of  $\beta$ -TrCP (Fig. 3b) and induction of PARP11 expression (Extended Data Fig. 3a). Notably, CRISPR/

**Fig. 1 | Downregulation of IFNAR1 in intratumoral CTLs undermines their activities.** **a**, Flow cytometry analysis of IFNAR1 levels on the surface of CD45 $^{+}$ CD3 $^{+}$ CD8 $^{+}$  T cells in spleen (Sp) and tumor (Tu) tissues from WT or SA mice on day 21 after inoculation of subcutaneous (s.c.) MC38 tumors ( $1 \times 10^6$  cells per mouse). Quantification data (right) are shown as mean  $\pm$  s.e.m. ( $n=6$  mice for each group). Statistical analysis was performed using ordinary one-way analysis of variance (ANOVA) with Tukey's multiple comparisons test. **b**, Immune cells were isolated from MC38 tumors growing in WT or SA mice on day 14 after inoculation.  $N=9,725$  cells were used for the single-cell RNA-seq analyses. A t-distributed stochastic neighbor embedding (t-SNE) plot of CD8 $^{+}$  T cells with clusters demarcated by colors demonstrating WT (blue,  $n=2,075$  cells) and SA (red,  $n=2,038$  cells). **c**, Gene set enrichment analysis (GSEA) of differentially expressed genes comparing CD8 $^{+}$  T cells in WT and SA groups. Black and red colors denote genesets enriched in WT and SA, respectively. NES, normalized enrichment score; NF- $\kappa$ B, nuclear factor  $\kappa$ B; TNF, tumor necrosis factor. **d**, Leading-edge plots showing results from GSEA of CD8 $^{+}$  T cell function in relevant genesets comparing CD8 $^{+}$  T cells in WT and SA groups. ES, enrichment score; FDR, false discovery rate. **e**, Dot plot showing expression of T cell exhaustion (underlined below) and function-related genes. The size of the dot corresponds to the percentage of cells expressing the gene in each group and the color represents the average expression level. WT,  $n=2,075$  cells; SA,  $n=2,038$  cells. **f**, t-SNE plot of CD8 $^{+}$  T cells with clusters demarcated by colors demonstrating seven clusters based on gene expression (as in Extended Data Fig. 1c). **g**, t-SNE plot analysis of proportion of CD8 $^{+}$  T cell clusters (as in f) in WT and SA samples. WT,  $n=2,075$  cells; SA,  $n=2,038$  cells. **h**, Flow cytometry analysis of IFN- $\gamma$ -positive CD8 $^{+}$  T cells in naive spleens and tumor tissues from mice of indicated genotypes. Data are shown as mean  $\pm$  s.e.m. (WT and SA spleen,  $n=5$  mice; WT and SA tumor,  $n=6$  mice). Statistical analysis was performed using ordinary one-way ANOVA with Tukey's multiple comparisons test. \*\* $P=0.0050$ ; NS, not significant.



Cas9-mediated knockout of either *Parp11* or p38 $\alpha$  (encoded by *Mapk14*) or of  $\beta$ -TrCP1/2 (encoded by *Fbxw1/Fbxw11*) prevented downregulation of IFNAR1 by adenosine (Extended Data Fig. 3b,c). The role of p38 $\alpha$ /*Mapk14* in intratumoral CTLs has been demonstrated<sup>19,27</sup>; therefore, we next focused on the importance of PARP11-mediated downregulation of IFNAR1.

PARP11 expression was induced upon exposure of CTLs to factors present in the tumor-conditioned medium (TCM) (Fig. 3c) and elevated in the intratumoral CTLs compared to those isolated from spleens (Fig. 3d). Furthermore, ADP ribosylation of  $\beta$ -TrCP in human T cells was increased by their exposure to adenosine (Fig. 3e). Similar result was seen in recombinant HA-tagged  $\beta$ -TrCP expressed in 293T cells (Extended Data Fig. 3d). Of note, a greater enzymatic activity in ADP ribosylation of Myc-tagged  $\beta$ -TrCP in vitro was facilitated by PARP11 purified from cells treated with adenosine (Fig. 3f). These results suggest that adenosine (and perhaps other factors present in the TME) increase expression and activity of PARP11.

Genetic evidence for the importance of PARP11 came from studies in *Parp11* knockout mice (Extended Data Fig. 3e and reported elsewhere<sup>34</sup>), whose CTLs maintained proper responses to adenosine as manifested by phosphorylation of protein kinase A and CREB transcription factor (Fig. 3g,h and Extended Data Fig. 3f). Yet these *Parp11*-null CTLs were deficient in adenosine-induced upregulation of  $\beta$ -TrCP (Fig. 3i). As expected, the inhibitor of A2AAR, CPI-444, prevented downregulation of IFNAR1 in response to adenosine but not to TCM (Fig. 3j and Extended Data Fig. 3g), which contains other stimuli capable of downregulating IFNAR1 such as inflammatory cytokines or extracellular vesicles<sup>22,23</sup>. Notably, knockout of *Parp11*-null stabilized IFNAR1 under both conditions (Fig. 3k and Extended Data Fig. 3g). Downregulation of IFNAR1 by adenosine was restored in *Parp11*-null CTLs upon re-expression of WT human PARP11 but not of catalytically inactive PARP11<sup>H3Ymu</sup> (H204P-Y236S) mutant (Fig. 3k and Extended Data Fig. 3h). In all, these results implicate PARP11-dependent ADP ribosylation in inactivation IFNAR1 in CTLs within the TME.

To determine the biological importance of this regulation, we analyzed tumor growth and CTL status in *Parp11* knockout mice. We found that the levels of IFNAR1 were greater in the intratumoral CTLs isolated from MC38 or B16F10 tumors growing in *Parp11*-null mice compared to those from WT hosts (Fig. 4a and Extended Data Fig. 4a). Furthermore, knockout of *Parp11* significantly delayed growth of these tumors as well as LLC (Fig. 4b,c and Extended Data Fig. 4b-d). Notably, ablation of PARP11 also notably increased the numbers (Fig. 4d and Extended Data Fig. 4e) and activity of intratumoral CTL as manifested by levels of IFN- $\gamma$ , CD69 and tumor necrosis factor (TNF)- $\alpha$  (Fig. 4e-g and Extended Data Fig. 4f-h). Of note, all these phenotypes observed in *Parp11*-null mice were

reversed in *Parp11*<sup>-/-</sup>*Ifnar1*<sup>-/-</sup> double knockout animals (Fig. 4 and Extended Data Fig. 4) suggesting a pivotal role of PARP11-driven downregulation of IFNAR1 in the TME for immune suppression and tumor growth.

**Targeting PARP11 improves the efficacy of CAR T cell therapy.** These results characterize PARP11 as an important negative immune regulator in the TME, and so we next focused on specific role of PARP11 in CTLs. Mining existing databases revealed PARP11 as one of the genes associated with CD8 $+$  T cell exhaustion<sup>35</sup>. Consistently, analysis of subsets of CD8 $+$  T cells from human patients with colorectal cancers<sup>36</sup> revealed that expression of PARP11 was decreased in a highly active effector CD103 $+$ CD39 $+$  subset (characterized by abundant expression of IFN- $\gamma$ , granzymes and perforin<sup>36</sup>) compared to effector memory or naive T cells (Fig. 5a). Together with our own results, these data support the rationale for targeting PARP11-driven ADP ribosylation to stabilize IFNAR1 and to increase the activity of therapeutic CTLs.

This rationale was first tested by manufacturing the CAR T cells from WT or PARP11-null T lymphocytes (Extended Data Fig. 5a). Notably, even upon exposure to adenosine, *Parp11*-deficient T cells harboring mesothelin-targeting (Meso) CAR (Extended Data Fig. 5b) maintained IFNAR1 levels (Fig. 5b) and tumoricidal activities (Fig. 5c). Similar effects of PARP11 inactivation were observed when CAR T cells from WT or *Parp11*-null mice were manufactured using CAR against CD19 antigen (Fig. 5d and Extended Data Fig. 5c). Of note, deletion of IFNAR1 reversed the effects of PARP11 ablation as was seen in CAR T cells derived from *Parp11*<sup>-/-</sup>*Ifnar1*<sup>-/-</sup> mice (Fig. 5d,e).

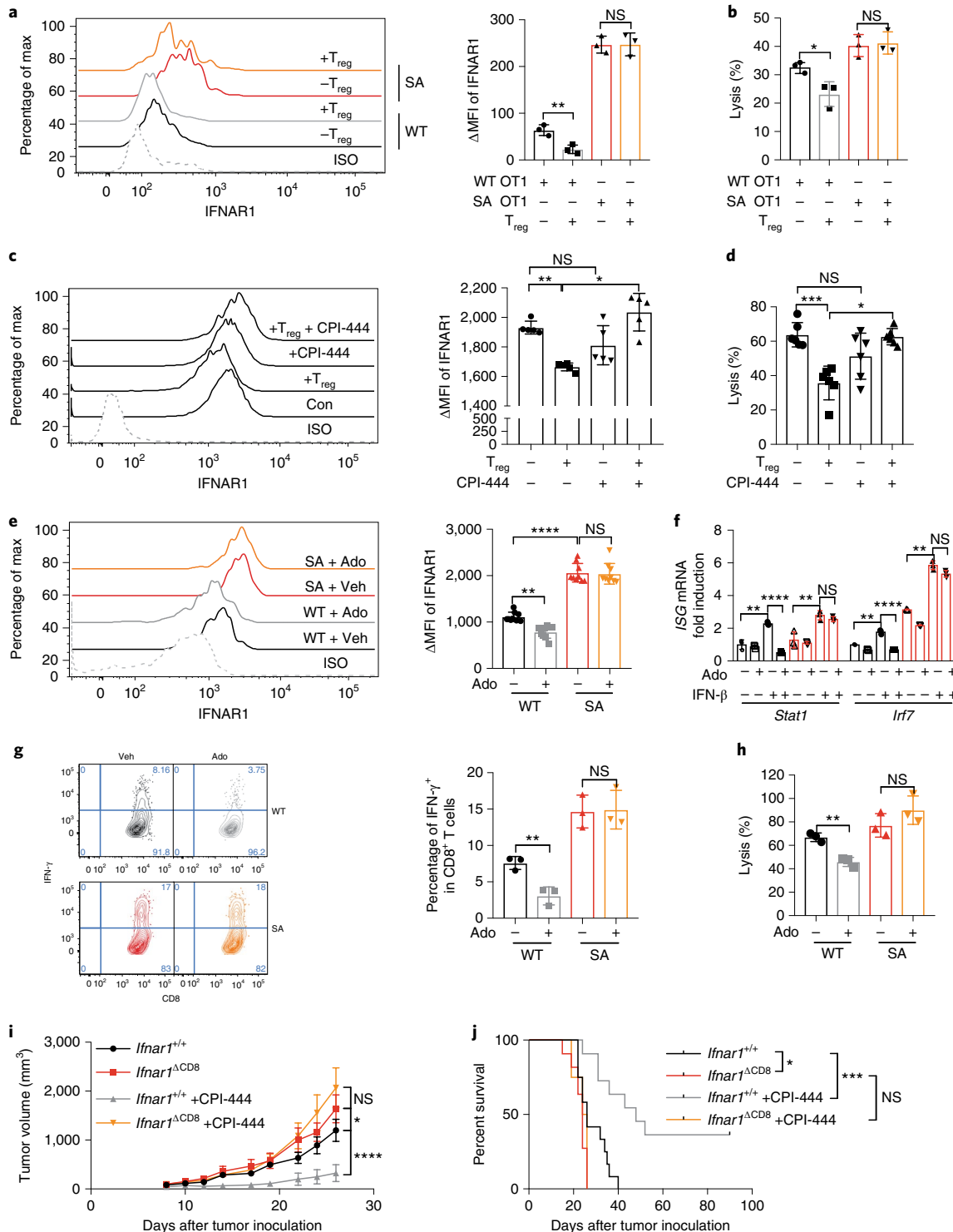
These results indicate that stabilization of IFNAR1 upon ablation of *Parp11* renders these cells resistant to the immunosuppressive effects of adenosine in vitro. Furthermore, the efficacy of anti-CD19 CAR T cells in vivo followed the same pattern (Fig. 5f,g and Extended Data Fig. 5d). Under these conditions, PARP11 status in CAR T cells did not affect the expression of CD19 antigen by malignant cells (Extended Data Fig. 5e). Ablation of PARP11 in CAR T cells decreased their cell surface levels of TIM-3 but not of PD-1 or LAG-3 exhaustion markers (Extended Data Fig. 5f) and increased CAR T cell persistence in blood and tumors but not in the spleen (Extended Data Fig. 5g). These results suggest that PARP11-driven inactivation of IFNAR1 in CTLs plays an important role in the immunosuppressive effects of the TME and provide a further rationale for targeting PARP11-driven ADP ribosylation to increase the efficacy of CAR T cell therapies.

Driven by these considerations, we engineered a fourth-generation anti-CD19 CAR that expressed a short hairpin RNA (shRNA) against *PARP11* (Fig. 6a). Transduction of human T cells with this construct downregulated *PARP11* (Extended Data Fig. 6a,b)

**Fig. 2 | Downregulation of CTL IFNAR1 by T<sub>reg</sub> cells and adenosine.** **a**, iT<sub>reg</sub> cells were co-cultured with OT-1 cells (T<sub>reg</sub>:OT-1 ratio was 1:3) for 24 h. Then, IFNAR1 on the surface of OT-1 cells were analyzed by flow cytometry. A two-tailed unpaired Student's t-test was used to analyze data; \*\*P=0.0085; n=3 co-cultures. **b**, Lysis of MC38OVA-Luc cells by WT or SA OT-1 cells co-cultured with iT<sub>reg</sub> cells at indicated conditions (T<sub>reg</sub>:OT-1 ratio was 1:3; E:T ratio was 10:1). Data were analyzed by two-tailed unpaired Student's t-test; \*P=0.0259; n=3 co-cultures. **c**, iT<sub>reg</sub> cells were co-cultured (T<sub>reg</sub>:OT-1 ratio was 1:3) with OT-1 cells ( $\pm$ CPI-444, 10  $\mu$ M 1 h). Then IFNAR1 on the surface of OT-1 cells was analyzed by flow cytometry. One-way ANOVA. \*\*P=0.0022; \*P=0.0416. n=5 co-cultures. **d**, Lysis of MC38OVA-Luc cells by OT-1 cells ( $\pm$ CPI-444, 10  $\mu$ M 1 h) co-cultured with iT<sub>reg</sub> cells at indicated conditions (T<sub>reg</sub>:OT-1 ratio was 1:3; E:T ratio was 10:1). Data were analyzed by one-way ANOVA; \*\*\*P=0.0002; \*P=0.0410; n=6 co-cultures. **e**, IFNAR1 on the surface of indicated CD8 $+$  T cells ( $\pm$ Ado, 1mM, 2 h). Data were analyzed by one-way ANOVA; \*\*P=0.0018; \*\*\*\*P<0.0001; n=9 mice. **f**, qPCR analysis of mRNA in the indicated mouse splenocytes pretreated with adenosine (Ado, 1mM) for 2 h and then stimulated with IFN- $\beta$  (1,000 IU ml $^{-1}$ ) for 16 h. Data were analyzed by one-way ANOVA; \*\*P<0.01; \*\*\*\*P<0.0001; n=3 mice. **g**, IFN- $\gamma$  levels in indicated CD8 $+$  T cells ( $\pm$ Ado, 1mM, 24 h). Data were analyzed by one-way ANOVA; \*\*P=0.0068; n=3 mice. **h**, Lysis of MC38OVA-luc cells by OT-1 cells ( $\pm$ Ado, 1mM 24 h). Data were analyzed by one-way ANOVA; \*\*P=0.0024; n=3 co-cultures. **i**, Growth of MC38 tumors (1 $\times$ 10 $6$  cells per mouse, s.c.) inoculated into WT (*Ifnar1*<sup>+/+</sup>) or *Ifnar1*<sup>ACD8</sup> mice and treated daily with CPI-444 (10 mg kg $^{-1}$ , oral gavage) or vehicle on days 1-12. *Ifnar1*<sup>+/+</sup>, *Ifnar1*<sup>ACD8</sup>, n=13 mice; *Ifnar1*<sup>+/+</sup>+CPI-444, n=7 mice; *Ifnar1*<sup>+/+</sup>+CPI-444, n=8 mice. Data were analyzed by two-way ANOVA; \*P=0.0364; \*\*\*\*P<0.0001. **j**, Kaplan-Meier analysis of survival from experiment described in **i** (*Ifnar1*<sup>+/+</sup>, n=12 mice; *Ifnar1*<sup>ACD8</sup>, n=11 mice; *Ifnar1*<sup>+/+</sup>+CPI-444, n=11 mice; *Ifnar1*<sup>ACD8</sup>+CPI-444, n=8 mice). Data were analyzed by log-rank (Mantel-Cox) test; \*P=0.0295; \*\*\*P=0.0008; NS, not significant.

and rendered these cells resistant to IFNAR1 downregulation by adenosine (Fig. 6b). CAR T cells manufactured with this construct (Extended Data Fig. 6c) maintained their tumoricidal activity against CD19-expressing cells (including naturally expressing CD19 NALM6 leukemia cells) even in the presence of adenosine (Fig. 6c,d). Notably, CAR modified to inactivate PARP11 also exhibited increased anti-tumorigenic efficacy in vivo (Fig. 6e,f) suggesting a therapeutic potential for genetic or pharmacologic inhibition of PARP11 to restore IFNAR1 function and reactivate CAR T cells.

These conclusions were further supported by a complementary approach of ablating PARP11 in human CAR T cells using CRISPR-Cas9 technology (Extended Data Fig. 6d-f). We used Meso CAR, which can target pancreatic, lung and ovarian cancer cells and exhibits a reasonable safety profile with potentially promising efficacy (reviewed elsewhere<sup>37</sup>). Knockout of PARP11 in these cells notably increased the efficacy of their adoptive transfer as manifested by deceleration of tumor growth (Fig. 6g) and prolonged animal survival (Fig. 6h).



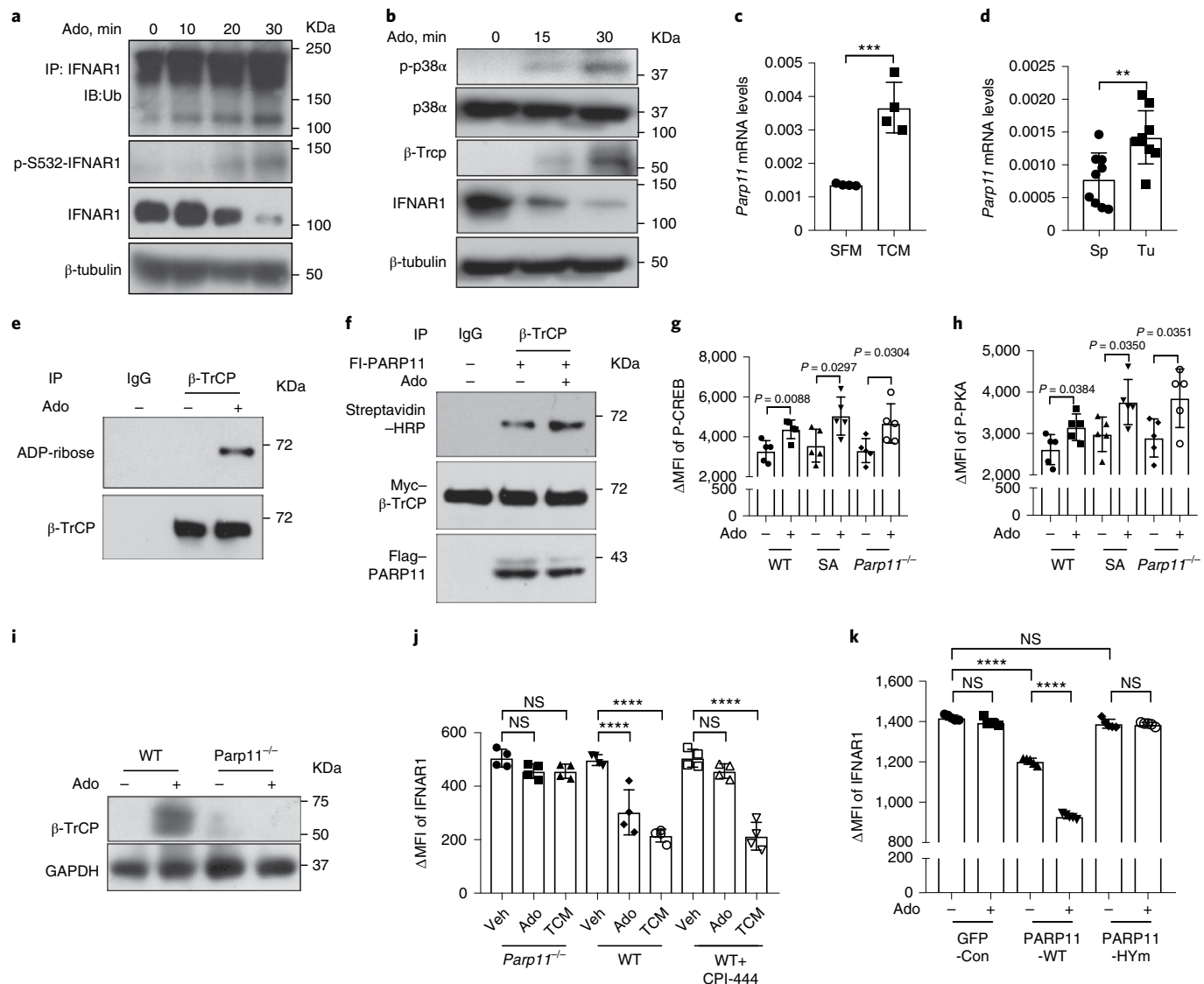


**Fig. 3 | PARP11 regulates IFNAR1 downregulation in CD8<sup>+</sup> T cells.** **a**, Immunoblot (IB) analysis of ubiquitination, phosphorylation and total levels of IFNAR1 in Jurkat cells treated with adenosine (Ado, 1mM) at the indicated time points. IP, immunoprecipitation. **b**, Immunoblot analysis of phosphorylation and levels of p38 $\alpha$  and levels of IFNAR1 and β-TrCP in Jurkat cells treated with adenosine (Ado, 1mM) at the indicated time points. Data are representative of three independent repeats with similar results (**a,b**). **c**, qPCR analysis of mRNA for *Parp11* in T cells treated with serum-free medium (SFM) or with TCM for 48 h. Data were analyzed by two-tailed unpaired Student's t-test; \*\*\*P=0.0009; n=4 mice. **d**, qPCR analysis of *Parp11* mRNA in CTLs isolated from tumors or spleens of MC38 tumor-bearing mice. Data were analyzed by two-tailed unpaired Student's t-test; \*\*P=0.004; Sp, n=9 mice; Tu, n=9 mice. **e**, ADP ribosylation of β-TrCP immunoprecipitated from human T cells treated or not with adenosine (1mM, 30 min) as indicated was analyzed by immunoblot. **f**, In vitro ADP ribosylation of Myc-β-TrCP immunoprecipitated with Myc or control antibody and incubated on beads with biotinylated NAD<sup>+</sup> in the presence of soluble Flag-PARP11 purified from 293T cells treated or not with adenosine (Ado, 1mM, 30 min) as indicated. Reactions were probed with streptavidin-HRP conjugate. Input levels of Myc-β-TrCP and Flag-PARP11 are also shown. Data are representative of three independent repeats with similar results (**e,f**). **g**, Flow cytometry analysis of phospho-CREB in (±Ado, 1mM, 2 h). Data were analyzed by one-way ANOVA; n=5 mice. **h**, Flow cytometry analysis of phospho-PKA in (±Ado, 1mM, 2 h). Data were analyzed by one-way ANOVA; n=5 mice. **i**, Immunoblot analysis of β-TrCP levels in indicated splenocytes treated with or without adenosine (Ado, 1mM, 30 min) as indicated. Data are representative of three independent repeats with similar results. **j**, Flow cytometry analysis of levels of IFNAR1 in indicated CTLs (±CPI-444, 10 μM, 1h) and then treated with adenosine (Ado, 1mM) or TCM as indicated for 2 h. Data were analyzed by one-way ANOVA; \*\*\*\*P<0.0001; n=4 mice. **k**, Flow cytometry analysis of levels of IFNAR1 in *Parp11*<sup>-/-</sup> CTL transduced with empty virus (GFP-con) or viruses for expression of human WT PARP11 or HYm PAPR11 mutant and treated with adenosine (Ado, 1mM, 2h). Data were analyzed by one-way ANOVA; \*\*\*\*P<0.0001; n=4 mice.

We then focused on a pharmacologic approach to provide a proof of principle for inhibiting ADP ribosylation to improve the efficacy of CAR T adoptive transfer therapies. We first targeted p38 kinase, whose genetic ablation improved the therapeutic efficacy of CAR T cells in an IFNAR1-dependent manner<sup>19,27</sup>. Treatment of Meso CAR T cells (Extended Data Fig. 7a) with the p38 inhibitor

ralimetinib (LY) prevented adenosine-induced IFNAR1 downregulation (Extended Data Fig. 7b) and robustly increased anti-tumorigenic activity of these CAR T cells in vitro (Extended Data Fig. 7c) and in vivo (Extended Data Fig. 7d,e).

As development of bioavailable PARP11-specific inhibitors is still in progress<sup>38</sup>, we took advantage of the fact that the US Food

and Drug Administration-approved drug rucaparib, which targets PARP1/2 (ref. <sup>39</sup>), is also capable of inhibiting PARP11 (ref. <sup>25</sup>). Rucaparib prevented induction of  $\beta$ -TrCP and downregulation of IFNAR1 by adenosine in human T cells (Fig. 7a). Of note, the antitumor effect of rucaparib in immunocompetent WT hosts harboring MC38 tumors was no longer evident in *Ifnar1*<sup>ACD8</sup> mice (Fig. 7b,c) indicating that stabilization of IFNAR1 in CTLs plays a key role in the mechanisms of action for rucaparib. Of note, rucaparib increased *in vivo* efficacy of WT but not of *Parp11*-null anti-CD19 CAR T cells (Fig. 7d) suggesting that modulation of PARP11 status by rucaparib significantly contributes to its antitumor effects.

Notably, addition of rucaparib preserved IFNAR1 levels (Fig. 7e) and tumoricidal activities (Fig. 7f) in adenosine-treated human Meso CAR T cells. Furthermore, combination of rucaparib with transfer of these Meso CAR T cells in immunocompromised mice harboring mesothelin-expressing tumors exhibited a significantly increased efficacy compared to monotherapy with either of these agents (Fig. 7g,h).

## Discussion

The studies described here support a mechanism that facilitates inactivation of CTLs and formation of the immune-privileged niche inside solid tumors. We demonstrate that PARP11, which is induced and hyperactivated in response to adenosine (and likely many other factors present in the TME), acts to stabilize  $\beta$ -TrCP, which in turn, facilitates accelerated ubiquitination and degradation of IFNAR1. This partial loss of IFNAR1 undermines the cytolytic activity of CTLs (this work) and decrease their viability<sup>19</sup>.

Findings presented here reveal that even a partial loss of IFNAR1 on intratumoral CTLs contributes to the immunosuppressive effects of adenosine and  $T_{reg}$  cells, whose ability to produce adenosine is important for their function<sup>40</sup>. The sequelae of IFNAR1 downregulation in CTLs include their decreased viability (likely due to inactivation of the interleukin-2 pathway<sup>19</sup>) and the impairment of tumoricidal activities demonstrated here. IFN1 provides a ‘third signal’ to support the clonal expansion of CD8<sup>+</sup> T cells<sup>16–18</sup>. Complete genetic ablation of IFNAR1 in antiviral CTLs interfered with their cytolytic activities<sup>41</sup>; however, even modest IFNAR1 downregulation on intratumoral CTLs was associated with decreased expression of cytolytic mediators and tumoricidal activity.

Such sensitivity of CTLs to high receptor density suggests that activation of CTLs by IFN1 represents a highly tunable type of effect (reviewed previously<sup>42</sup>) and, hence, could be modulated for therapeutic purposes. Both IFNAR1 phosphorylation and expression of  $\beta$ -TrCP E3 ligase are required for efficient IFNAR1 ubiquitination and downregulation<sup>12</sup>. Accordingly, targeting either p38 kinase or the PARP11– $\beta$ -TrCP axis significantly improved tumoricidal activities of CTLs in the TME.

Adenosine did not affect the levels of  $\beta$ -TrCP mRNA in CTLs. Thus, it is plausible that adenosine elicits stabilization of  $\beta$ -TrCP protein by stimulating expression and catalytic activity of PARP11.

As a result, increased PARP11-dependent mono-ADP ribosylation of  $\beta$ -TrCP will protect this protein from ubiquitination and subsequent proteasomal degradation<sup>25</sup> otherwise facilitated by its partner proteins within SCF– $\beta$ -TrCP E3 ubiquitin ligase<sup>33</sup>. In turn, stabilized  $\beta$ -TrCP facilitates rapid downregulation of IFNAR1 (ref. <sup>25</sup>). Additional studies will test this possibility; however, it is also important not to rule out that other elements and conditions of the immunosuppressive TME may further contribute via upregulating  $\beta$ -TrCP mRNA. The latter can be induced by Wnt ligands<sup>24</sup>, which are excessively secreted by nonmalignant components of the TME<sup>43</sup>.

Future studies will help to understand the mechanisms underlying the induction and activation of PARP11 in the intratumoral T cells by tumor-derived factors; however, the findings presented here highlight the importance of PARP11-mediated inactivation of CTLs as a major driving force for immunosuppression in the TME. Inactivation of PARP11 and ensuing degradation of  $\beta$ -TrCP is expected to stabilize IFNAR1 and improve CTL activities under exposure to many TME factors and conditions thereby making this approach advantageous over specific inhibitors of adenosine signaling.

In the context of developing more-efficient CAR T cells, inactivation of PARP11 or/and p38 is technologically more advantageous than the expression of the stabilized IFNAR1<sup>SA</sup> mutant, which causes unfolded protein response<sup>44</sup> and restricts proliferation of T cells (Fig. 1 and reported elsewhere<sup>19</sup>). Furthermore, restoring the sensitivity to IFN1 specifically in T cells might be important because hyperactivation of the IFN pathways in malignant cells promotes tumor growth and undermines the efficacy of immunotherapies<sup>45,46</sup>. This effect in malignant cells probably contributes to a paradoxical role of IFNAR1 in CAR T cells when these are combined with oncolytic virus producing massive amounts of IFN1 in the TME<sup>47</sup>.

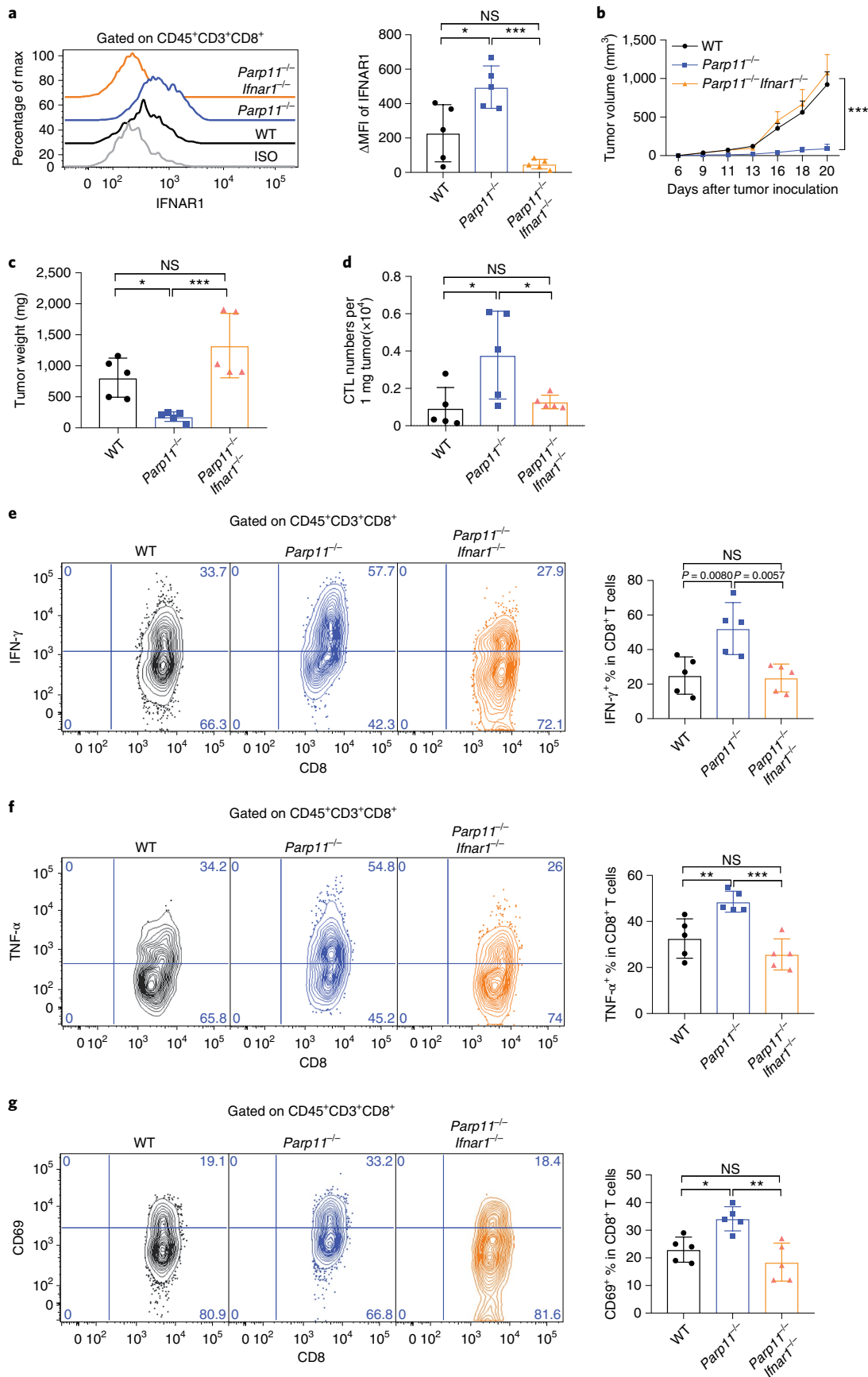
Promising results have been reported for combination of already available ADP ribosylation inhibitors (including rucaparib) with immune-checkpoint blocking agents (reviewed elsewhere<sup>48</sup>). Within this context, our findings warrant a prompt development of potent, selective and bioavailable PARP11 inhibitors and add an impetus to clinical trials that combine such agents with immune and other types of anticancer therapies.

Furthermore, along with the lack of suitable antigenic targets, immunosuppressive effects of the TME are considered to be the major mechanism of resistance of solid tumors to CAR T cell therapy (reviewed previously<sup>37</sup>). This study provides a clear rationale for new approaches to CAR engineering and combinatorial therapeutic regimens with the goal of targeting ADP ribosylation and downregulation of IFNAR1 to increase the efficacy of CAR T cell therapy in solid tumors.

## Methods

**Study approvals.** Use of human T cells that were previously collected from healthy donors under informed consent and could not be directly or indirectly linked to individual human participants was approved for the Human Immunology Core by the Institutional Review Board of the University of Pennsylvania. All animal experiments were approved by the Institutional Animal Care and Use Committee

**Fig. 4 | Inactivation of intratumoral CTLs and robust tumor growth require IFNAR1-dependent function of PARP11 in the TME.** **a**, Flow cytometry analysis of levels of IFNAR1 on the surface of CD45<sup>+</sup>CD3<sup>+</sup>CD8<sup>+</sup> T cells in tumor tissues from WT, *Parp11*<sup>−/−</sup> and *Parp11*<sup>−/−</sup>/*Ifnar1*<sup>−/−</sup> mice 20 d after inoculation of s.c. MC38 tumors (0.5 × 10<sup>6</sup> cells per mouse). Quantification is shown (right). Statistical analysis was performed using ordinary one-way ANOVA with Tukey’s multiple comparisons test; \*P = 0.011, \*\*P = 0.0002; n = 5 mice. **b**, Volume of MC38 s.c. tumors in mice of indicated genotypes. Statistical analysis was performed using two-way ANOVA with Tukey’s multiple comparisons test; \*\*\*P = 0.0009; n = 5 mice. **c**, Tumor weight of MC38 tumors grown in mice of indicated genotypes (day 20). Statistical analysis was performed using ordinary one-way ANOVA with Tukey’s multiple comparisons test; \*P = 0.0387, \*\*\*P = 0.0007; n = 5 mice. **d**, Flow cytometry analysis of numbers of CD8<sup>+</sup> T cells in MC38 tumors growing in indicated mice. Statistical analysis was performed using ordinary one-way ANOVA with Tukey’s multiple comparisons test; \*P < 0.05; n = 5 mice. **e**, Flow cytometry analysis of IFN-γ<sup>+</sup> cells gated on CD45<sup>+</sup>CD3<sup>+</sup>CD8<sup>+</sup> T cells isolated from MC38 tumors grown in indicated mice. Statistical analysis was performed using ordinary one-way ANOVA with Tukey’s multiple comparisons test; \*\*P < 0.01; n = 5 mice. **f**, Flow cytometry analysis of TNF-α<sup>+</sup> cells gated on CD45<sup>+</sup>CD3<sup>+</sup>CD8<sup>+</sup> T cells isolated from MC38 tumors grown in indicated mice. Statistical analysis was performed using ordinary one-way ANOVA with Tukey’s multiple comparisons test; \*\*P = 0.0081, \*\*\*P = 0.0005; n = 5 mice. **g**, Flow cytometry analysis of CD69<sup>+</sup> cells gated on CD45<sup>+</sup>CD3<sup>+</sup>CD8<sup>+</sup> T cells isolated from MC38 tumors grown in indicated mice. Statistical analysis was performed using ordinary one-way ANOVA with Tukey’s multiple comparisons test; \*P = 0.0164, \*\*P = 0.0016; n = 5 mice.



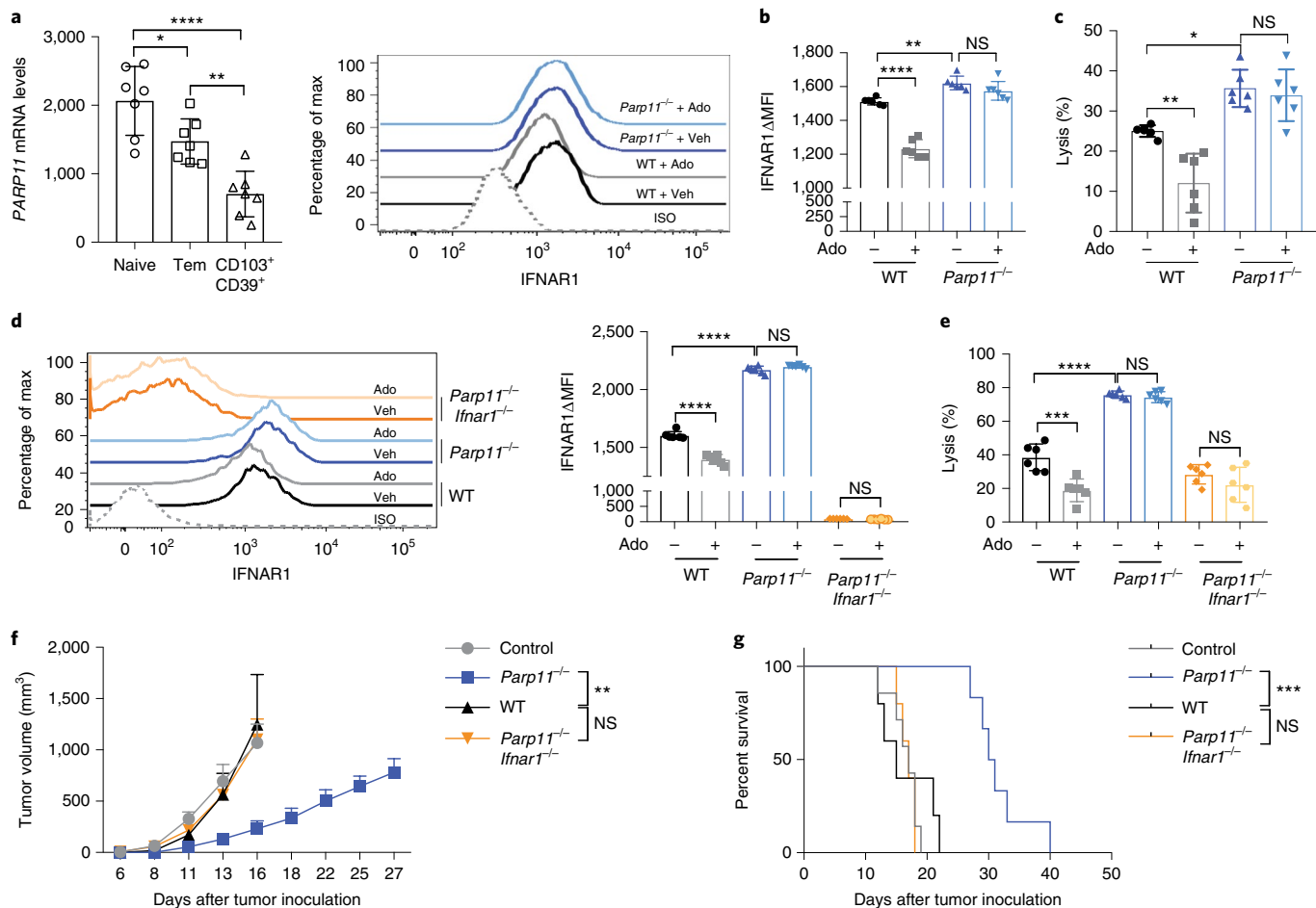


**Fig. 5 | PARP11 undermines tumoricidal activities of CAR T cells.** **a**, Relative expression of PARP11 in CD8<sup>+</sup> T cell subsets isolated from patients with colorectal cancer<sup>36</sup>. Data in naive, effector memory and highly active effector CD103<sup>+</sup>CD39<sup>+</sup> subpopulations are shown. Statistical analysis was performed using ordinary one-way ANOVA with Tukey's multiple comparisons test; \*P=0.0312, \*\*\*P<0.0001, \*\*P=0.0052; n=7 samples. **b**, Flow cytometry analysis of the IFNAR1 levels on indicated Meso-BBz CAR T cells treated with or without Ado (Ado, 1mM, 24 h). Statistical analysis was performed using ordinary one-way ANOVA with Tukey's multiple comparisons test; \*\*\*P<0.0001, \*\*P=0.0021; n=6 independently treated cell cultures. BBz, contains the intracellular 4-1BB co-stimulatory and CD3ζ signaling domains. **c**, Lysis of EM-Meso-GFP-Luc cells by Meso-BBz CAR T cells produced from WT and *Parp11*<sup>-/-</sup> mice treated as indicated (E:T ratio of 10:1). Statistical analysis was performed using ordinary one-way ANOVA with Tukey's multiple comparisons test; \*\*P<0.0027, \*P=0.0144; n=6 independently treated cell cultures. **d**, Flow cytometry analysis of the IFNAR1 levels on CD19-BBz CAR T cells produced from WT, *Parp11*<sup>-/-</sup> and *Parp11*<sup>-/-</sup>/*Ifnar1*<sup>-/-</sup> mice treated as indicated. Statistical analysis was performed using ordinary one-way ANOVA with Tukey's multiple comparisons test; \*\*\*P<0.0001; n=5 mice. **e**, Lysis of hCD19-B16F10 cells by CD19-BBz CAR T cells produced from WT, *Parp11*<sup>-/-</sup> and *Parp11*<sup>-/-</sup>/*Ifnar1*<sup>-/-</sup> mice treated as indicated (E:T ratio of 10:1). Statistical analysis was performed using ordinary one-way ANOVA with Tukey's multiple comparisons test; \*\*\*P=0.0002, \*\*\*\*P<0.0001; n=6 independently treated cell cultures. **f**, Tumor growth (s.c.) of hCD19-B16F10 tumor-bearing C57BL/6 mice adoptively transferred with CD19-BBz CAR T cells (2×10<sup>6</sup> per mouse, i.v. at day 7) as indicated. Statistical analysis was performed using two-way ANOVA with Tukey's multiple comparisons test; \*\*P=0.0019; control, n=7 mice, *Parp11*<sup>-/-</sup>, n=6 mice; WT, n=5 mice, *Parp11*<sup>-/-</sup>/*Ifnar1*<sup>-/-</sup>, n=5 mice. **g**, Kaplan-Meier analysis of survival of animals from experiment described in **f**. Statistical analysis was performed using Gehan-Breslow-Wilcoxon test; \*\*\*P=0.0007; control, n=7 mice, *Parp11*<sup>-/-</sup>, n=6 mice; WT, n=5 mice, *Parp11*<sup>-/-</sup>/*Ifnar1*<sup>-/-</sup>, n=5 mice.

of the University of Pennsylvania and were carried out in accordance with the guidelines.

**Animal studies.** All mice had water ad libitum and were fed regular chow. Mice were maintained in a specific-pathogen-free facility in accordance with American Association for Laboratory Animal Science guidelines. Mice were housed in single-sex cages at 20±2°C under a 12-h light–12-h dark photoperiod with the lights on at 07:00. C57BL/6 littermate *Ifnar1*<sup>+/+</sup> (“WT”) and *Ifnar1*<sup>S526A</sup> mice (SA) have been described previously; the SA mice were donated to Jackson Laboratories and are available from this source (C57BL/6-*Ifnar1*<sup>tm1.1Sypf</sup>/J; stock no. 035564). As described previously, *Parp11* knockout mice exhibited teratozoospermia and male infertility but otherwise developed normally and did not display any overt pathology<sup>34</sup>.

*Ifnar1*<sup>-/-</sup> mice (B6(Cg)-*Ifnar1*<sup>tm1.2Ees</sup>/J; stock no. 028288), *Ifnar1*<sup>fl/fl</sup> mice (B6(Cg)-*Ifnar1*<sup>tm1.1Ees</sup>/J, stock no. 028256), C57BL/6-Tg(Cd8a-cre)1Itan/J (CD8-cre, stock no. 008766) and NOD.Cg-*Prkdc*<sup>scid</sup> *Il2rg*<sup>tm1Wjl</sup>/*SzJ* (NSG, stock no. 005557)

mice were purchased from the Jackson Laboratory. CD8-cre mice were crossed with *Ifnar1*<sup>fl/fl</sup> mice to generate CD8-cre::*Ifnar1*<sup>+/+</sup> (WT) mice and CD8-cre::*Ifnar1*<sup>fl/fl</sup> (*Ifnar1*<sup>ΔCD8</sup>) littermates. All these mice were viable and fertile with no reported abnormalities. The genotyping PCR primers are provided in Supplementary Table 1. Littermate animals from different cages were randomly assigned into the experimental groups. These randomized experimental cohorts were either co-housed or systematically exposed to the bedding of other groups to ensure equal exposure to the microbiota of all groups.

**Reagents and constructs.** Adenosine (Sigma, A4036), TGF-β (R&D 7666-MB-005/CF), prostaglandin E2 (PGE2, Sigma, P0409), rucaparib (Selleckchem, S1098) and CPI-444 (Medkoo Biosciences, 206848) were purchased. Retroviral vectors for transduction of PARP11-null CTL with control (GFP-Con) virus or viruses for expression of WT or catalytically inactive HYmu PARP11 mutant was carried out as described elsewhere<sup>25</sup>.

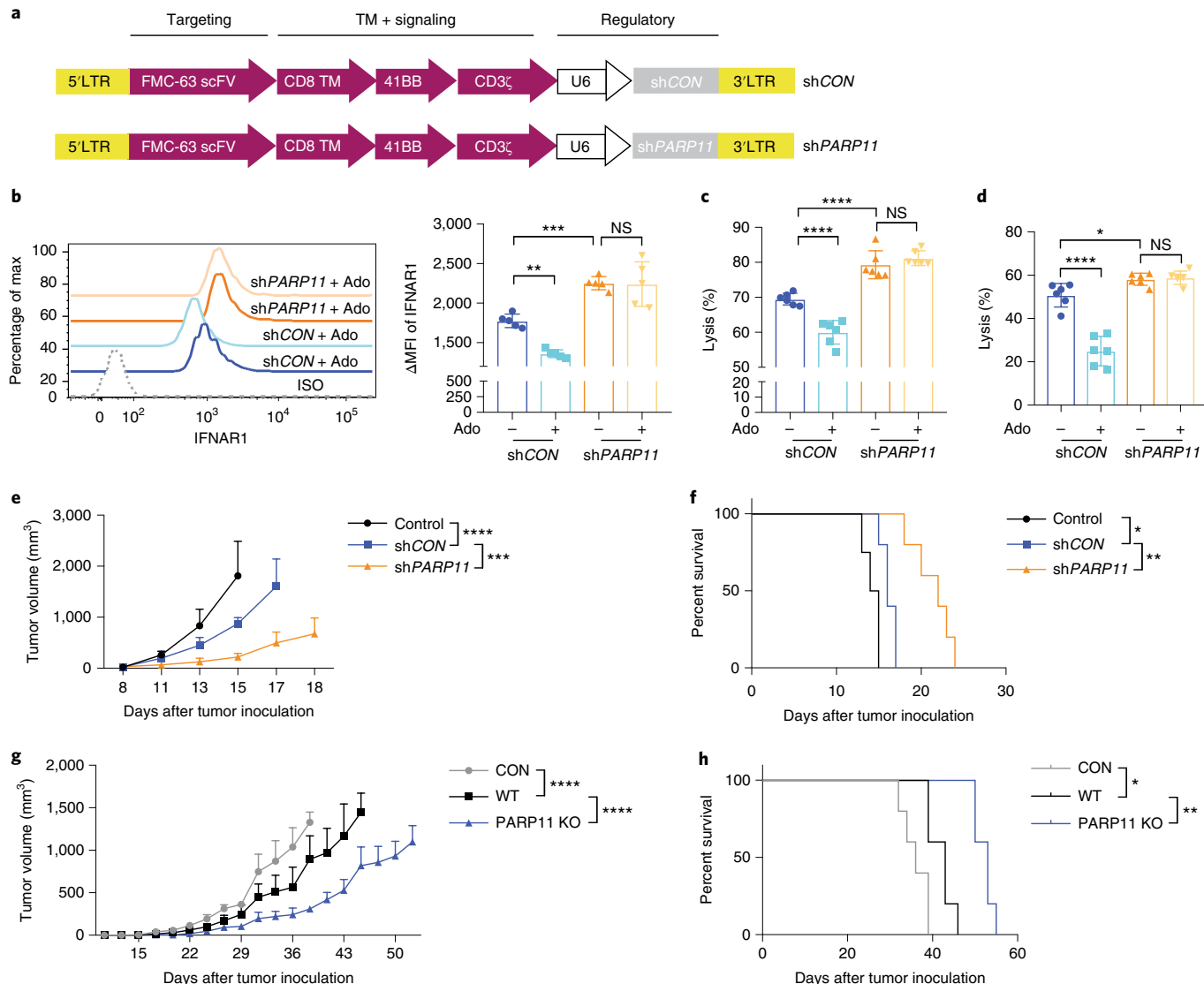


**Fig. 6 | Increased efficacy of CAR T cells engineered to inactivate PARP11.** **a**, Schematic representation of shCON and shPARP11-CD19-BBz chimeric receptors. sh, short hairpin. **b**, Flow cytometry analysis of levels of IFNAR1 on the surface of indicated CAR T cells treated with or without adenosine (Ado, 1 mM, 24 h). Statistical analysis was performed using ordinary one-way ANOVA with Tukey's multiple comparisons test; \*\*P = 0.0033, \*\*\*P = 0.0009; n = 5 samples. **c**, Lysis of hCD19-B16F10 cells by shCON-CD19-BBz or shPARP11-CD19-BBz CAR T cells treated with or without adenosine (Ado, 1 mM, 24 h). (E:T ratio was 10:1). Statistical analysis was performed using ordinary one-way ANOVA with Tukey's multiple comparisons test; \*\*\*P < 0.0001; n = 6 independently treated cell cultures. **d**, Lysis of NALM6 cells that express endogenous CD19 by shCON-CD19-BBz or shPARP11-CD19-BBz CAR T cells treated with or without adenosine (Ado, 1 mM, 24 h) (E:T ratio was 10:1). Statistical analysis was performed using ordinary one-way ANOVA with Tukey's multiple comparisons test; \*\*\*P < 0.0001, \*P = 0.0426; n = 6 independently treated cell cultures. **e**, hCD19-B16F10 tumor growth in NSG mice inoculated with  $5 \times 10^5$  hCD19-B16 cells (s.c.) and 7 d later administered with indicated CAR T cells ( $1 \times 10^6$  per mouse, intravenously (i.v.)). Statistical analysis was performed using two-way ANOVA with Tukey's multiple comparisons test; \*\*\*\*P < 0.0001, \*\*\*P = 0.0005; Con, n = 4 mice; shCon, n = 5 mice; shPARP11, n = 5 mice. **f**, Kaplan-Meier analysis of survival of animals from experiment described in **e** (Con, n = 4 mice; shCon, n = 5 mice; shPARP11, n = 5 mice). Statistical analysis was performed using log-rank (Mantel-Cox) test; \*P = 0.0138, \*\*P = 0.0026. **g**, Growth of EM-Meso-GFP-Luc tumors ( $1 \times 10^6$  per mouse, s.c.) in NSG mice that were administered with control (PBS) or WT or PARP11 knockout Meso-BBz CAR T cells ( $1 \times 10^6$  per mouse, i.v. on day 7). Statistical analysis was performed using two-way ANOVA with Tukey's multiple comparisons test; \*\*\*\*P < 0.0001; n = 5 mice. **h**, Kaplan-Meier analysis of survival of animals from experiment described in Fig. 6g. Statistical analysis was performed using log-rank (Mantel-Cox) test; \*\*P = 0.0019, \*P = 0.0174; n = 5 mice.

**Cell lines and tumor-conditioned medium preparation.** Mouse cell lines MC38, B16F10, LLC and EL4 and human Jurkat, NALM6 and 293T cells were purchased from the American Type Culture Collection and maintained according to their recommendations. Mouse B16F10 cells bearing human CD19 (hCD19-B16F10) were generated by transduction and subsequent selection. The mouse MC38OVA and human EM-Meso-GFP-Luc cell lines were generously provided by S. Ostrand-Rosenberg (University of Maryland) and by E. Moon (University of Pennsylvania), respectively. MC38OVA and hCD19-B16F10 cells were further

engineered to stably express firefly luciferase. EM-Meso-GFP-Luc cells were maintained in DMEM (Gibco) supplemented with 10% FBS (HyClone) and 100 U ml<sup>-1</sup> penicillin-streptomycin (Gibco). TCM was prepared as previously described<sup>19</sup>. For in vitro treatments, we used SFM or TCM added to complete medium at a 3:1 ratio.

**Tumor models.** MC38, B16F10 and LLC tumors were s.c. injected into the right flank of the indicated syngeneic mice. EM-Meso-GFP-Luc and hCD19-B16F10

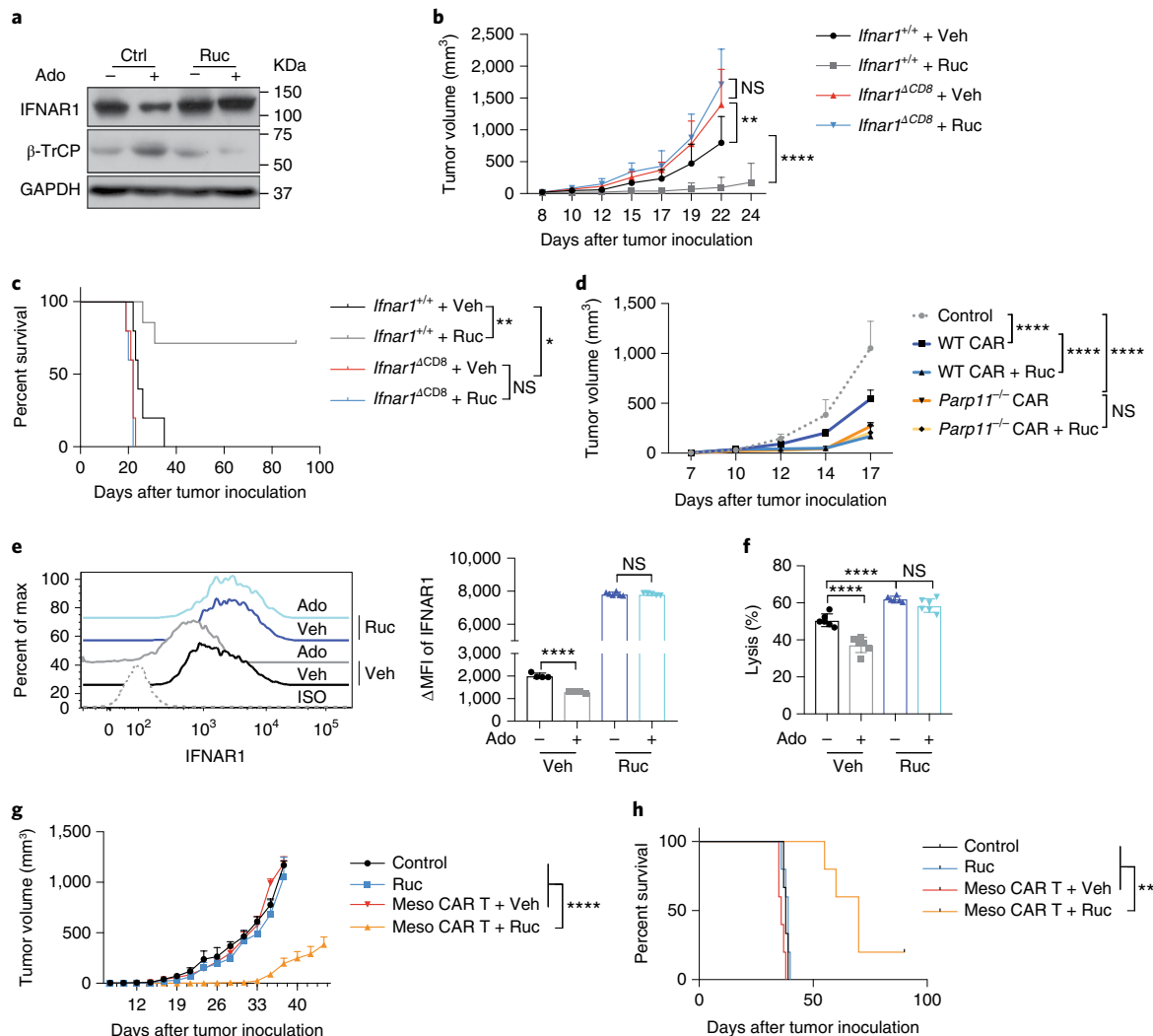


**Fig. 7 | Rucaparib increases the efficacy of CAR T cell therapies.** **a**, Immunoblot analysis of  $\beta$ -TrCP and IFNAR1 levels in Jurkat cells ( $\pm$  Ruc, 1 $\mu$ M, 2 h) and then treated with or without adenosine (Ado, 1 mM) for 30 min. Data are representative of three independent repeats with similar results. **b**, Volume of MC38 tumors ( $5 \times 10^5$  cells per mouse, s.c.) in Ifnar1<sup>+/+</sup> and Ifnar1<sup>ΔCD8</sup> mice that were administered with rucaparib (Ruc) at 40 mg kg<sup>-1</sup> or vehicle (Veh) every other day from day 7. Data were analyzed by two-way ANOVA; \*\*P = 0.0034, \*\*\*\*P < 0.0001; Ifnar1<sup>+/+</sup> + Veh, Ifnar1<sup>ΔCD8</sup> + Veh and Ifnar1<sup>ΔCD8</sup> + Ruc; n = 5 mice; Ifnar1<sup>+/+</sup> + Ruc, n = 7 mice. **c**, Kaplan-Meier analysis of survival from **b**. Data were analyzed by log-rank (Mantel-Cox) test; \*\*P = 0.0046, \*P = 0.0230; Ifnar1<sup>+/+</sup> + Veh, Ifnar1<sup>ΔCD8</sup> + Veh and Ifnar1<sup>ΔCD8</sup> + Ruc, n = 5 mice; Ifnar1<sup>+/+</sup> + Ruc, n = 7 mice. **d**, Growth of hCD19-B16F10 tumors ( $5 \times 10^5$  cells per mouse, s.c.) in NSG mice that were administered with WT or Parp1<sup>-/-</sup> CD19-BBz CAR T cells ( $10^6$  per mouse, i.v. at day 7) and Ruc (20 mg kg<sup>-1</sup> by oral gavage at day 10, 12 and 14) or Veh. Data were analyzed by two-way ANOVA; \*\*\*\*P < 0.0001; n = 5 mice. **e**, IFNAR1 levels on Meso-BBz CAR T ( $\pm$  Ruc, 10  $\mu$ M, 72 h) and treated with or without adenosine (Ado, 1 mM, 24 h). Data were analyzed by two-tailed unpaired Student's t-test; \*\*\*\*P < 0.0001; Veh treated with or without Ado, n = 4 independently treated cell cultures; Ruc treated with Veh, n = 6 independently treated cell cultures; Ruc treated with Ado, n = 5 independently treated cell cultures. **f**, Killing efficacy of human Meso-BBz CAR T ( $\pm$  Ruc, 10  $\mu$ M, 72 h), then treated with adenosine (Ado, 1 mM, 24 h) co-cultured with EM-Meso-GFP-Luc cells (E:T ratio 10:1). Data were analyzed by one-way ANOVA; \*\*\*\*P < 0.0001; n = 6 independently treated cell cultures. **g**, Growth of EM-Meso-GFP-Luc tumors ( $1 \times 10^6$  cells per mouse, s.c.) in NSG mice that were administered with 0.5  $\times$  10<sup>6</sup> Meso-BBz CAR T cells (i.v.) on day 7 and rucaparib (40 mg kg<sup>-1</sup>) or vehicle every other day from day 7 for six times. Data were analyzed by two-way ANOVA; \*\*\*\*P < 0.0001; control, n = 3 mice; Ruc, Meso CAR T + Veh, Meso CAR T + Ruc, n = 5 mice. **h**, Kaplan-Meier analysis of survival from **g**. Data were analyzed by log-rank (Mantel-Cox) test; \*\*P < 0.01; control, n = 3 mice; Ruc, Meso CAR T + Veh, Meso CAR T + Ruc, n = 5 mice.

were s.c. injected into the right flank of NSG mice. Tumor volumes were measured using caliper three times per week starting at day 7 after inoculation. The maximal tumor size was 1,000 mm<sup>3</sup> and was not exceeded.

**Human or mouse CAR T cells preparation.** Human or mouse T cells were activated with magnetic beads precoated with agonist antibodies against CD3 and CD28 (Gibco) according to the instructions. Then human T cells were transduced with CD19-BBz or Meso-BBz CAR at day 1 and expanded for 10 d or collected at specific time points for analysis. Mouse T cells were spin transduced CD19-BBz or Meso-BBz CAR at day 2 and expanded for 5 d for in vitro or in vivo function studies.

**scRNA-seq analysis.** scRNA-seq libraries were prepared following protocol from Chromium Controller 10X Genomics and then sequenced using Illumina Nextseq 550. BCL files were generated for further analysis. Alignment, filtering, barcode counting and unique molecular identifier counting were performed using Cell Ranger v.4.0.0 (<https://support.10xgenomics.com/single-cell-gene-expression/software/overview/welcome>). Data were further analyzed using Seurat v.3.1.5 (<https://satijalab.org/seurat/>). Cells with at least 500 detected genes, at least 1,000 detected RNAs and no more than 50,000 RNAs were included in downstream analyses. Raw unique molecular identifier counts were normalized to unique molecular identifier count per million total counts and log transformed, using a

NormalizeData function. Data were scaled with regression to nCount RNA and group (WT versus SA), using ScaleData function. Variable genes were selected based on average expression and dispersion. Principal-component analysis was performed with default settings. Clusters and t-SNE plots were generated based on selected principal-component analysis dimensions. t-SNE plots and dot plots showing the expression of labeled genes were performed using FeaturePlot and DotPlot functions. Differential gene expression analysis was performed using FindMarkers function with following parameters: min.cells.group, 1; min.cells.feature, 1; min.pct, 0; logfc.threshold, 0; and only.pos, FALSE. The resultant output (ave\_logFC) was utilized as input for GSEA with a pre-rank mode. Data have been submitted to the Gene Expression Omnibus under accession no. [GSE171055](#).

**Flow cytometry analysis.** Tumors or spleens were collected and incubated in dissociation solution with 2 mg ml<sup>-1</sup> Collagenase II (MP Biomedicals) or 1 mg ml<sup>-1</sup> Collagenase IV (Roche) plus 100 µg ml<sup>-1</sup> DNase I (Roche) for 1 h with continuous agitation. Cells were filtered using a 70-µm cell strainer and resuspended with FACS buffer (PBS with 1% BSA and 1 mM EDTA). Isolated cells were incubated with anti-mouse CD16/CD32 antibody (BioLegend, Clone 93, cat. no. 101302, 1:50 dilution) for 15 min on ice to block nonspecific Fc receptor binding. Cells were then stained with cell surface markers for 30 min on ice. For FOXP3 intracellular staining, cells were stained according to recommendations of the manufacturer of the eBioscience Foxp3/Transcription Factor Staining Buffer Set (cat. no. 00-5523-00). For intracellular staining, cells were stimulated with phorbol myristate acetate, ionomycin and Golgi-stop for 6 h as described elsewhere<sup>19</sup>. The flow antibodies are listed in Supplementary Table 2. Samples were acquired by LSRFortessa flow cytometry (FACS Diva software v.7, BD Biosciences). Data were analyzed with FlowJo software (FlowJo v.9.9.6, BD Biosciences).

Immunoprecipitation, immunoblot, ubiquitination and ADP ribosylation assays were carried out as previously described<sup>23,25</sup>. For analysis of IFNAR1 ubiquitination, anti-IFNAR1 EA12 antibody (10 µg per sample) was added to 500 µg protein cell lysate and incubated with rotation at 4 °C overnight. The protein G-Sepharose beads were added to the supernatant for 4 h. The immunocomplexes were washed three times with lysis buffer and then analyzed by immunoblot using mono- and polyubiquitylated conjugates monoclonal antibody (FK2) (Enzo Life Sciences). Polyclonal antibody against phospho-Ser532-IFNAR1 (ref. <sup>50</sup>) and monoclonal antibody for immunoprecipitation of human IFNAR1 (EA12 (ref. <sup>51</sup>)) were previously described.

Mono-ADP ribosylation of β-TrCP (immunoprecipitated using antibody against β-TrCP or HA tag) was detected by western blotting using ADP ribosylation antibody (Millipore, MABE1075).

The in vitro ADP ribosylation assay was carried out as previously described. Briefly, 293T cells were transfected with Myc-β-TrCP or Flag-PARP11 expression vectors. Forty-eight hours after transfection, cells expressing Flag-PARP11 were treated with adenosine (1 mM, 30 min) or PBS.

Whole-cell lysates were subjected to immunoprecipitation with anti-Myc beads or FLAG (M2) beads, respectively. Flag-PARP11 was then eluted with FLAG peptide (Sigma). The eluted Flag-PARP11 was incubated with beads-immobilized Myc-β-TrCP or control IgG immunoprecipitated in the presence of 100 µM Biotin-NAD<sup>+</sup> in 50 mM Tris-HCl buffer (pH 7.4) for 1 h at room temperature. ADP ribosylation of Myc-β-TrCP was detected by western blotting using streptavidin-HRP after SDS-PAGE.

The commercially available antibodies are listed in Supplementary Table 2.

**Quantitative PCR.** Total RNA was extracted using Trizol reagent (Invitrogen). The High-Capacity RNA-to-cDNA kit (Applied Biosystems) was used to make complementary DNA. Real-time PCR was performed using SYBR Green Master Mix reagents (Applied Biosystems). The expression of each gene was calculated based on the cycle threshold, set within the linear range of DNA amplification. The relative expression was calculated by the cycle threshold method, with normalization of raw data to a housekeeping gene. The primer sequences are provided in Supplementary Table 3.

#### Differentiation of iT<sub>reg</sub> cells and isolation of T<sub>reg</sub> cells from tumor tissues.

Mouse iT<sub>reg</sub> cells were differentiated from naïve CD4<sup>+</sup> T cells using the commercial CellXVivo T<sub>reg</sub> cell differentiation kits (CDK007, R&D). Briefly, naïve CD4<sup>+</sup> T cells were isolated from mice spleens and activated by plate-coated anti-CD3 (10 µg ml<sup>-1</sup>), anti-CD28 (2 µg ml<sup>-1</sup>) antibodies in the presence of TGF-β (10 ng ml<sup>-1</sup>) and interleukin-2 (2 ng ml<sup>-1</sup>) for 5–7 d. The yield and purity of T<sub>reg</sub> fraction was monitored by analysis of CD4<sup>+</sup>Foxp3<sup>+</sup> cells using flow cytometry. iT<sub>reg</sub> cells were not restimulated before co-culture with the target cells.

Intratumoral T<sub>reg</sub> cells were isolated from MC38 tumors grown in WT mice using MACS separation kit (Miltenyi Biotec). Isolated T<sub>reg</sub> cells were co-cultured with OT-1 cells at a ratio of 1:3 and the OT-1 cell toxicity was determined as described in the next section.

**Cytotoxicity assays.** The ability of CTL (including OT-1, Meso-BBz CAR T cells or CAR T-hCD19-BBz cells) to kill target cells expressing luciferase and either OVA or mesothelin or hCD19 was evaluated in a luciferase-based cytotoxicity assay. Target cells were co-cultured with CTL at the indicated E:T ratios in 96-well

black plate at a total volume of 200 µl. Target cells alone were seeded in parallel at the same density to quantify the spontaneous death luciferase expression ('relative luminescent units (RLU); spontaneous death RLU'). Target cells lysed with water were considered as the maximal killing ('maximal killing RLU'). Following co-culture, 100 µl of luciferase substrate (Bright-Glo; Promega) was added to the remaining supernatant and cells. Luminescence was measured after a 10-min incubation using the EnVision (PerkinElmer) plate reader. The percent cell lysis was obtained using the following calculation: Percentage lysis of 100 × (spontaneous death RLU – test RLU) / (spontaneous death RLU – maximal killing RLU).

**Chemical inhibitors in vivo treatment.** A2AR inhibitor CPI-444 (Medkoo Biosciences, 206848) was dissolved in 40% hydroxypropyl β-cyclodextrin and administered by oral gavage from day 1 at the dose of 10 mg kg<sup>-1</sup> daily for 12 d after MC38 inoculation. PARP inhibitor rucaparib (Selleckchem, S1098) were dissolved in 5% dimethylsulfoxide (DMSO) + 30% PGE300 + 10% Tween80 and administered by oral gavage at the dose of 20 mg kg<sup>-1</sup> or 40 mg kg<sup>-1</sup> every other day from day 7 after MC38 inoculation.

**CRISPR-Cas9-mediated gene knock outs.** We used the Cas9 lentivirus to infect EL4 cells and selected by blasticidin. Then single-guide RNA (sgRNA) lentivirus for indicated genes was added to infect Cas9-EL4 and selected by puromycin. The sgRNA sequences are listed in Supplementary Table 4.

To CRISPR out PARP11 in human T cells, primary T cells were stimulated with Dynabeads Human T cell expander CD3/CD28 (Invitrogen) (T cells:beads at 1:3 ratio) for 24 h and transduced with sgRNA lentivirus (lentiCRISPR v2, Addgene) and Meso CAR virus. At 24 h later, T cells were selected by puromycin, collected on day 7 and then utilized for the in vitro and in vivo studies. The sgRNA sequences are listed in Supplementary Table 4.

**Statistics and reproducibility.** Littermate animals from different cages were randomly assigned to the experimental groups. These randomized experimental cohorts were either co-housed or systematically exposed to the bedding of other groups to ensure equal exposure to the microbiota of all groups. Data collection and analysis were not performed blind to the conditions of the experiments. All described results are representative of at least three independent experiments unless specifically stated otherwise. Statistical analyses and the number of samples (*n*) were described in detail for each figure panel. No statistical method was used to predetermine sample size. No data were excluded from the analyses. Data were presented as average ± s.e.m. Statistical analysis was performed using Excel (Microsoft) or GraphPad Prism 8 software (GraphPad). A two-tailed unpaired Student's *t*-test was used for the comparison between two groups. One-way ANOVA or two-way ANOVA followed by the Tukey's test was used for the multiple comparisons. Repeated-measures two-way ANOVA (mixed model) followed by the Tukey's multiple comparisons test was used for analysis of the tumor growth curve. Kaplan-Meier curves were used to depict the survival function from lifetime data for mice and human patients; the log-rank (Mantel-Cox) test or Gehan-Breslow-Wilcoxon test was used to analyze the differences between the groups. A value of *P* < 0.05 was considered significant; \**P* < 0.05; \*\**P* < 0.01; \*\*\**P* < 0.001; \*\*\*\**P* < 0.0001; NS, not significant.

**Reporting summary.** Further information on research design is available in the Nature Research Reporting Summary linked to this article.

#### Data availability

Mouse scRNA-seq data are all available on the Gene Expression Omnibus (accession no. [GSE171055](#)). Source data have been provided as Source Data files. All other data supporting the findings of this study are available from the corresponding author on reasonable request. Source data are provided with this paper.

Received: 11 July 2021; Accepted: 22 April 2022;

Published online: 30 May 2022

#### References

- Jhunjhunwala, S., Hammer, C. & Delamarre, L. Antigen presentation in cancer: insights into tumour immunogenicity and immune evasion. *Nat. Rev. Cancer* **21**, 298–312 (2021).
- O'Donnell, J. S., Teng, M. W. L. & Smyth, M. J. Cancer immunoediting and resistance to T cell-based immunotherapy. *Nat. Rev. Clin. Oncol.* **16**, 151–167 (2019).
- Swann, J. B. & Smyth, M. J. Immune surveillance of tumors. *J. Clin. Invest.* **117**, 1137–1146 (2007).
- Hanahan, D. & Coussens, L. M. Accessories to the crime: functions of cells recruited to the tumor microenvironment. *Cancer Cell* **21**, 309–322 (2012).
- Joyce, J. A. & Fearon, D. T. T cell exclusion, immune privilege, and the tumor microenvironment. *Science* **348**, 74–80 (2015).
- Liu, C., Workman, C. J. & Vignali, D. A. Targeting regulatory T cells in tumors. *FEBS J.* **283**, 2731–2748 (2016).

7. Veglia, F. & Gabrilovich, D. I. Dendritic cells in cancer: the role revisited. *Curr. Opin. Immunol.* **45**, 43–51 (2017).
8. Vijayan, D., Young, A., Teng, M. W. L. & Smyth, M. J. Targeting immunosuppressive adenosine in cancer. *Nat. Rev. Cancer* **17**, 709–724 (2017).
9. Allard, B., Allard, D., Buisseret, L. & Stagg, J. The adenosine pathway in immuno-oncology. *Nat. Rev. Clin. Oncol.* **17**, 611–629 (2020).
10. Smyth, M. J., Ngiow, S. F., Ribas, A. & Teng, M. W. Combination cancer immunotherapies tailored to the tumour microenvironment. *Nat. Rev. Clin. Oncol.* **13**, 143–158 (2016).
11. Sharma, P. & Allison, J. P. Immune checkpoint targeting in cancer therapy: toward combination strategies with curative potential. *Cell* **161**, 205–214 (2015).
12. Fuchs, S. Y. Hope and fear for interferon: the receptor-centric outlook on the future of interferon therapy. *J. Interferon Cytokine Res.* **33**, 211–225 (2013).
13. Parker, B. S., Rautela, J. & Hertzog, P. J. Antitumour actions of interferons: implications for cancer therapy. *Nat. Rev. Cancer* **16**, 131–144 (2016).
14. Zitvogel, L., Galluzzi, L., Kepp, O., Smyth, M. J. & Kroemer, G. Type I interferons in anticancer immunity. *Nat. Rev. Immunol.* **15**, 405–414 (2015).
15. Bencic, J. L. et al. Tumor interferon signaling regulates a multigenic resistance program to immune checkpoint blockade. *Cell* **167**, 1540–1554 (2016).
16. Aichele, P. et al. CD8 T cells specific for lymphocytic choriomeningitis virus require type I IFN receptor for clonal expansion. *J. Immunol.* **176**, 4525–4529 (2006).
17. Curtsinger, J. M., Valenzuela, J. O., Agarwal, P., Lins, D. & Mescher, M. F. Type I IFNs provide a third signal to CD8 T cells to stimulate clonal expansion and differentiation. *J. Immunol.* **174**, 4465–4469 (2005).
18. Hervas-Stubbs, S. et al. Effects of IFN- $\alpha$  as a signal-3 cytokine on human naïve and antigen-experienced CD8(+) T cells. *Eur. J. Immunol.* **40**, 3389–3402 (2010).
19. Katlinski, K. V. et al. Inactivation of interferon receptor promotes the establishment of immune privileged tumor microenvironment. *Cancer Cell* **31**, 194–207 (2017).
20. Bhattacharya, S. et al. Anti-tumorigenic effects of Type 1 interferon are subdued by integrated stress responses. *Oncogene* **32**, 4214–4221 (2013).
21. Bhattacharya, S. et al. Triggering ubiquitination of IFNAR1 protects tissues from inflammatory injury. *EMBO Mol. Med.* **6**, 384–397 (2014).
22. Ortiz, A. et al. An Interferon-driven oxysterol-based defense against tumor-derived extracellular vesicles. *Cancer Cell* **35**, 33–45 e36 (2019).
23. Huangfu, W. C. et al. Inflammatory signaling compromises cell responses to interferon- $\alpha$ . *Oncogene* **31**, 161–172 (2012).
24. Spiegelman, V. S. et al. Wnt/ $\beta$ -catenin signaling induces the expression and activity of  $\beta$ TrCP ubiquitin ligase receptor. *Mol. Cell* **5**, 877–882 (2000).
25. Guo, T. et al. ADP-ribosyltransferase PARP11 modulates the interferon antiviral response by mono-ADP-ribosylating the ubiquitin E3 ligase  $\beta$ -TrCP. *Nat. Microbiol.* **4**, 1872–1884 (2019).
26. Bhattacharya, S. et al. Role of p38 protein kinase in the ligand-independent ubiquitination and down-regulation of the IFNAR1 chain of type I interferon receptor. *J. Biol. Chem.* **286**, 22069–22076 (2011).
27. Gurusamy, D. et al. Multi-phenotype CRISPR-Cas9 screen identifies p38 kinase as a target for adoptive immunotherapies. *Cancer Cell* **37**, 818–833 (2020).
28. Alicea-Torres, K. et al. Immune suppressive activity of myeloid-derived suppressor cells in cancer requires inactivation of the type I interferon pathway. *Nat. Commun.* **12**, 1717 (2021).
29. Josefowicz, S. Z., Lu, L. F. & Rudensky, A. Y. Regulatory T cells: mechanisms of differentiation and function. *Annu. Rev. Immunol.* **30**, 531–564 (2012).
30. Kumar, K. G. et al. Site-specific ubiquitination exposes a linear motif to promote interferon- $\alpha$  receptor endocytosis. *J. Cell Biol.* **179**, 935–950 (2007).
31. Kumar, K. G., Krolewski, J. J. & Fuchs, S. Y. Phosphorylation and specific ubiquitin acceptor sites are required for ubiquitination and degradation of the IFNAR1 subunit of type I interferon receptor. *J. Biol. Chem.* **279**, 46614–46620 (2004).
32. Kumar, K. G. et al. SCF(HOS) ubiquitin ligase mediates the ligand-induced down-regulation of the interferon- $\alpha$  receptor. *EMBO J.* **22**, 5480–5490 (2003).
33. Li, Y., Gazdoui, S., Pan, Z. Q. & Fuchs, S. Y. Stability of homologue of Slimb F-box protein is regulated by availability of its substrate. *J. Biol. Chem.* **279**, 11074–11080 (2004).
34. Meyer-Ficca, M. L. et al. Spermatid head elongation with normal nuclear shaping requires ADP-ribosyltransferase PARP11 (ARTD11) in mice. *Biol. Reprod.* **92**, 80 (2015).
35. Khan, O. et al. TOX transcriptionally and epigenetically programs CD8(+) T cell exhaustion. *Nature* **571**, 211–218 (2019).
36. Yang, R. et al. Distinct epigenetic features of tumor-reactive CD8<sup>+</sup> T cells in colorectal cancer patients revealed by genome-wide DNA methylation analysis. *Genome Biol.* **21**, 2 (2019).
37. Larson, R. C. & Maus, M. V. Recent advances and discoveries in the mechanisms and functions of CAR T cells. *Nat. Rev. Cancer* **21**, 145–161 (2021).
38. Kirby, I. T. et al. A potent and selective PARP11 inhibitor suggests coupling between cellular localization and catalytic activity. *Cell Chem. Biol.* **25**, 1547–1553 (2018).
39. Slade, D. PARP and PARG inhibitors in cancer treatment. *Genes Dev.* **34**, 360–394 (2020).
40. Maj, T. et al. Oxidative stress controls regulatory T cell apoptosis and suppressor activity and PD-L1-blockade resistance in tumor. *Nat. Immunol.* **18**, 1332–1341 (2017).
41. Kohlmeier, J. E., Cookenham, T., Roberts, A. D., Miller, S. C. & Woodland, D. L. Type I interferons regulate cytolytic activity of memory CD8(+) T cells in the lung airways during respiratory virus challenge. *Immunity* **33**, 96–105 (2010).
42. Pielher, J., Thomas, C., Garcia, K. C. & Schreiber, G. Structural and dynamic determinants of type I interferon receptor assembly and their functional interpretation. *Immunol. Rev.* **250**, 317–334 (2012).
43. Anastas, J. N. & Moon, R. T. WNT signalling pathways as therapeutic targets in cancer. *Nat. Rev. Cancer* **13**, 11–26 (2013).
44. Liu, J. et al. Virus-induced unfolded protein response attenuates antiviral defenses via phosphorylation-dependent degradation of the type I interferon receptor. *Cell Host Microbe* **5**, 72–83 (2009).
45. Minn, A. J. & Wherry, E. J. Combination cancer therapies with immune checkpoint blockade: convergence on interferon signaling. *Cell* **165**, 272–275 (2016).
46. Minn, A. J. Interferons and the immunogenic effects of cancer therapy. *Trends Immunol.* **36**, 725–737 (2015).
47. Evgin, L. et al. Oncolytic virus-derived type I interferon restricts CAR T cell therapy. *Nat. Commun.* **11**, 3187 (2020).
48. Peyraud, F. & Italiano, A. Combined PARP inhibition and immune checkpoint therapy in solid tumors. *Cancers* **12**, 1502 (2020).
49. Cho, C. et al. Cancer-associated fibroblasts downregulate type I interferon receptor to stimulate intratumoral stromagenesis. *Oncogene* **39**, 6129–6137 (2020).
50. Bhattacharya, S. et al. Inducible priming phosphorylation promotes ligand-independent degradation of the IFNAR1 chain of type I interferon receptor. *J. Biol. Chem.* **285**, 2318–2325 (2010).
51. Goldman, L. A. et al. Characterization of antihuman IFNAR-1 monoclonal antibodies: epitope localization and functional analysis. *J. Interferon Cytokine Res.* **19**, 15–26 (1999).

## Acknowledgements

This work was supported by the by the National Institutes of Health (NIH)/National Cancer Institute R01 grants CA247803 (to S.Y.F. and D.P.B.), R01 CA240814 (to S.Y.F. and A.B.) and P01 CA165997 grant (to J.A.D., C.K. and S.Y.F.), NIH/NICHD grant R15 HD100970 (to R.G.M.), NIH/NIA grant R56 AG069745 (to M.M.F.), K08 CA252619 (to M.J.A.) and National Natural Science Foundation of China (31970846 for Hui Z.). We thank staff at the Human Immunology Core at the University of Pennsylvania for providing purified human leukocyte subsets for our research. We are grateful to S. Ostrand-Rosenberg (University of Maryland) and E. Moon (University of Pennsylvania) for providing reagents. We greatly appreciate technical advice from A. Phan, L. Shallberg and A. Rotolo (University of Pennsylvania). We also thank D. Gabrilovich (Astra-Zeneca), A. Gamero (Temple University) and the members of the Fuchs, Minn and Koumenis Ryeom laboratories for critical suggestions.

## Author contributions

S.Y.F., H. Zhang, H. Zheng, M.C.M., A.J.M., J.A.D. and C.K. designed the research. H. Zhang, P.Y., V.S.T., X.C., M.J.A., Z.L., H.-G.Z., S.L., A.O., J.G., N.A.L., F.Y., A.B., D.P.B., J.L., S.N.-C., R.S.O., L.R.J. and S.G. directly performed the experiments and interpreted the data. M.L.M.-F. and R.G.M. provided key resources and valuable advice. S.Y.F., H. Zhang, H. Zheng, A.J.M., M.J.A., M.C.M., A.B., J.A.D. and C.K. wrote the manuscript with the help of all authors.

## Competing interests

The authors declare no competing interests.

## Additional information

**Extended data** is available for this paper at <https://doi.org/10.1038/s43018-022-00383-0>.

**Supplementary information** The online version contains supplementary material available at <https://doi.org/10.1038/s43018-022-00383-0>.

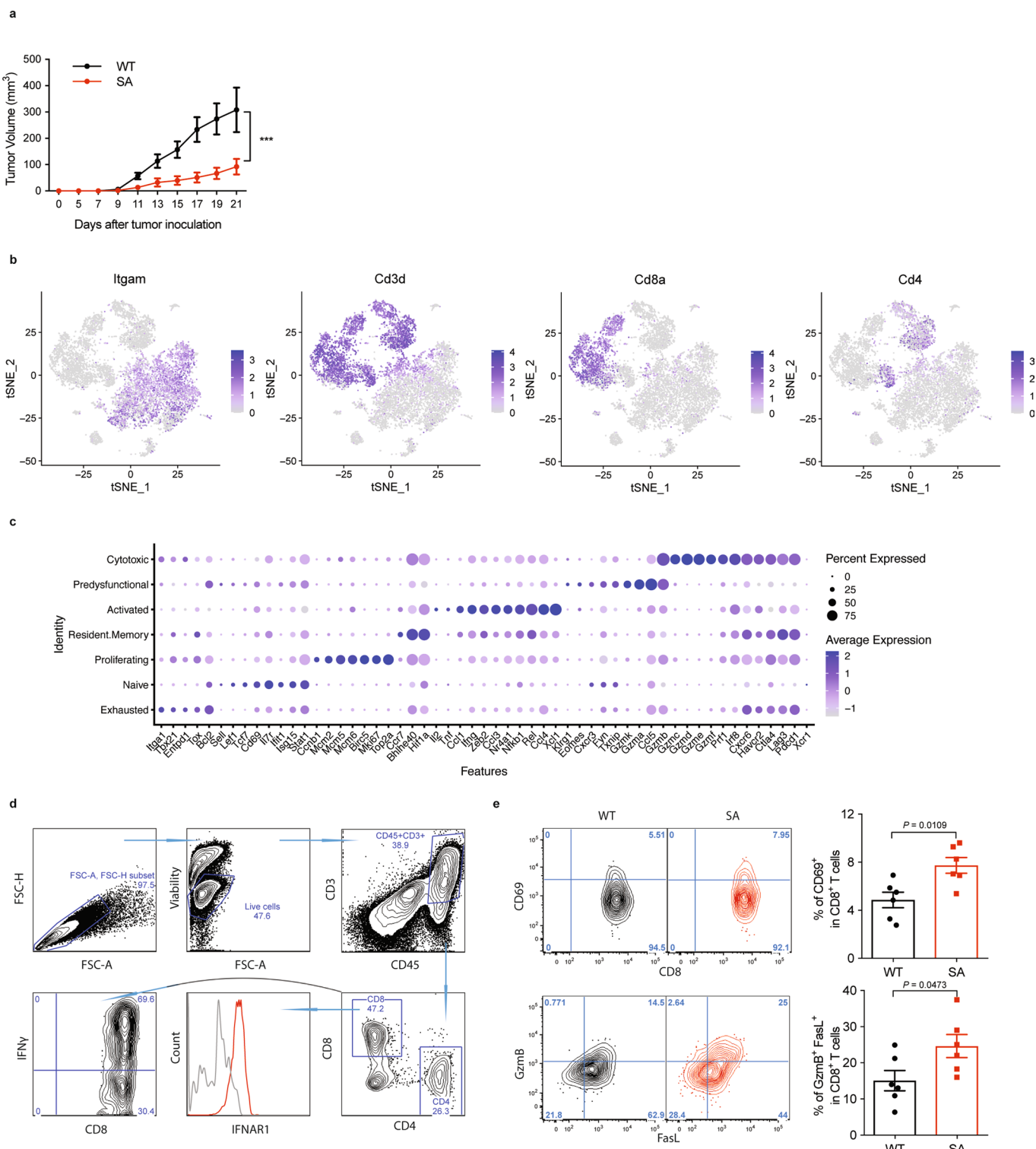
**Correspondence and requests for materials** should be addressed to Serge Y. Fuchs.

**Peer review information** *Nature Cancer* thanks the anonymous reviewers for their contribution to the peer review of this work.

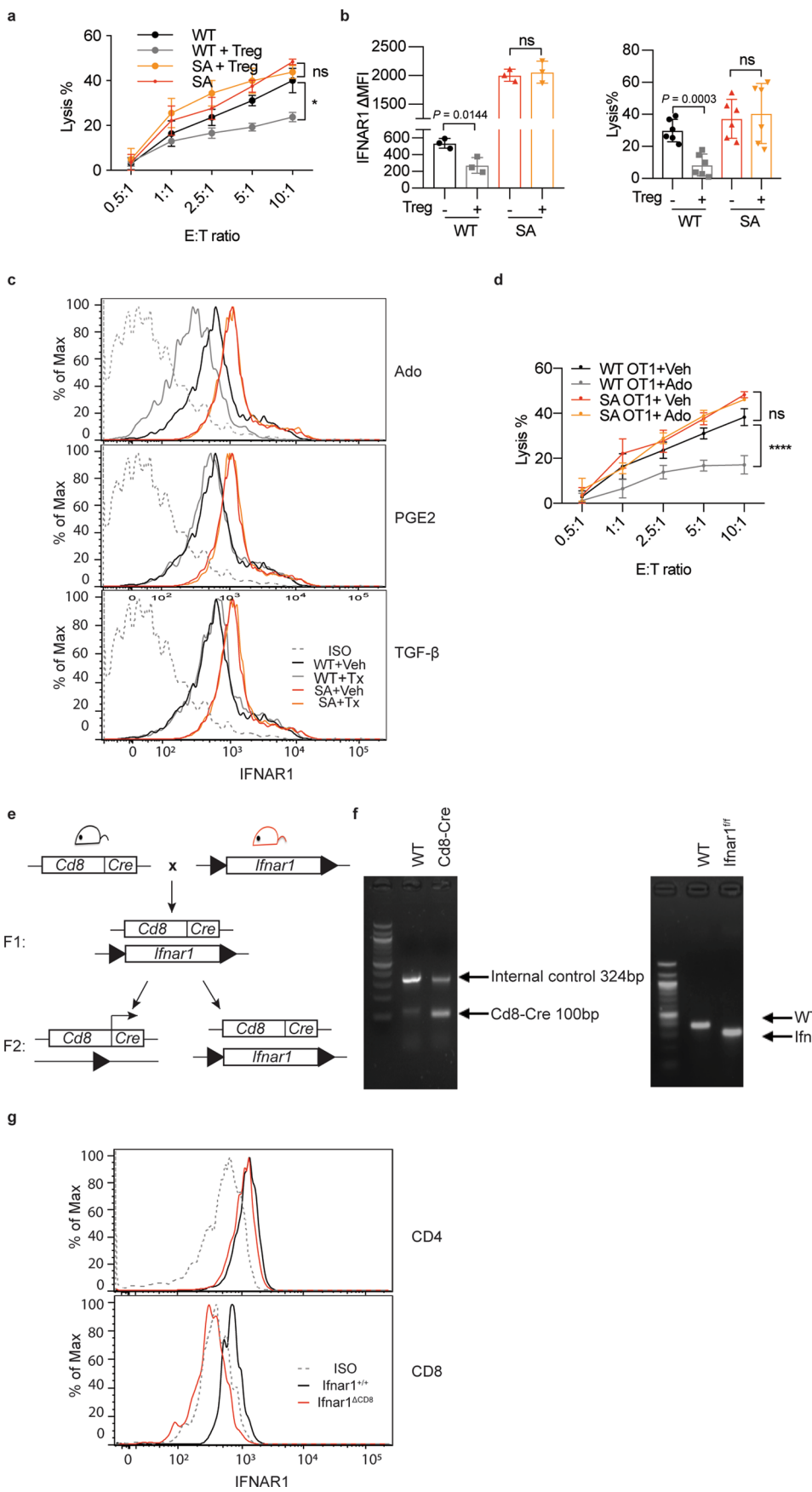
**Reprints and permissions information** is available at [www.nature.com/reprints](http://www.nature.com/reprints).

**Publisher's note** Springer Nature remains neutral with regard to jurisdictional claims in published maps and institutional affiliations.

© The Author(s), under exclusive licence to Springer Nature America, Inc. 2022

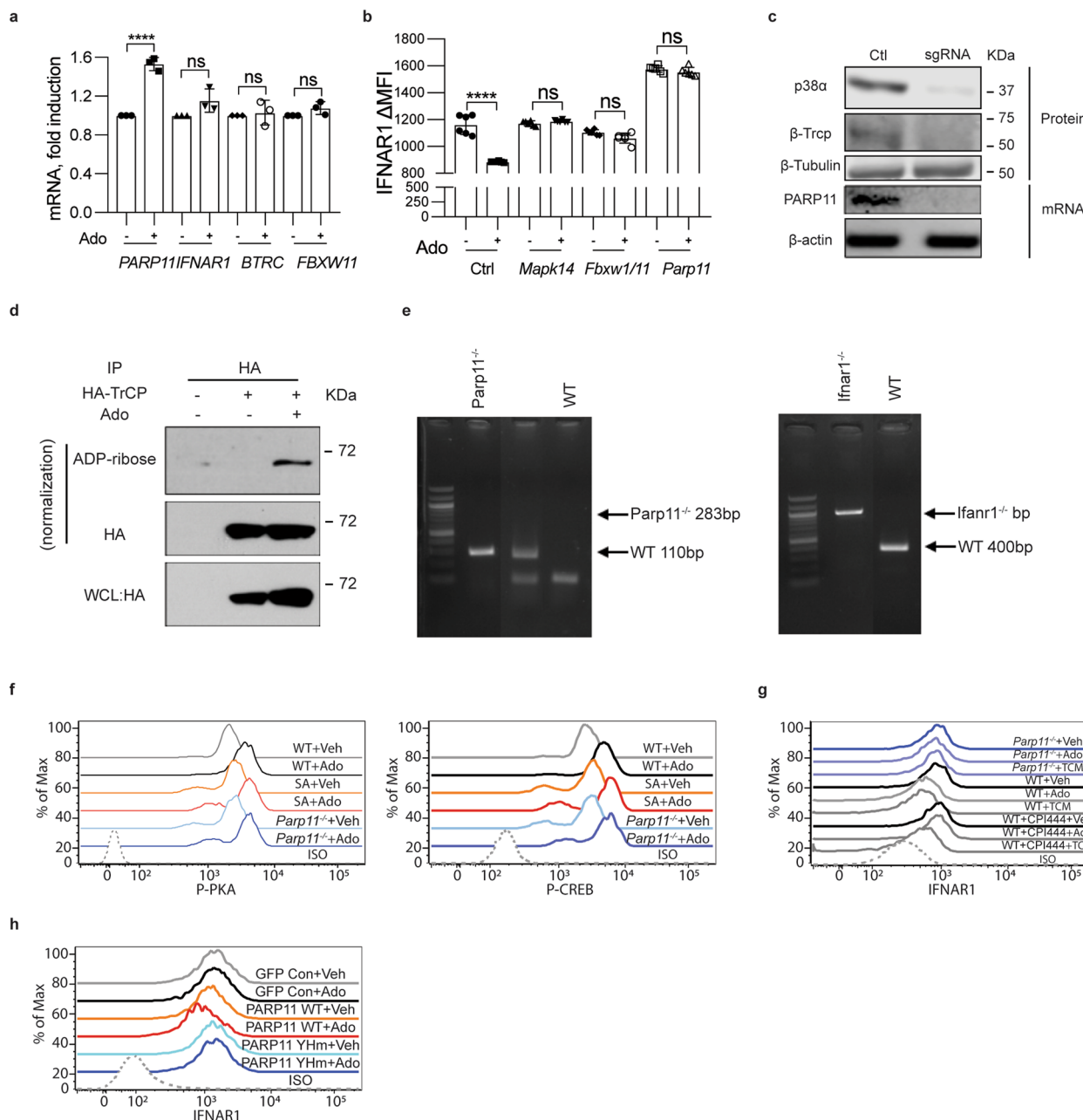


**Extended Data Fig. 1 | Downregulation of IFNAR1 on the intratumoral CTL undermines their activities.** **a** Growth of MC38 tumors ( $1 \times 10^6$ /mouse) after s.c. injection into WT and SA mice. Tumor volumes were measured 3 times per week. Data are shown as mean  $\pm$  SEM (WT, n=8 mice; SA, n=5 mice). Statistical analysis was performed using two-way ANOVA with Tukey's multiple comparisons test. \*\*\*P = 0.0004. **b** t-SNE plots showing the expression of *Itgam*, *Cd3d*, *Cd8a* and *Cd4*. Transcript levels are color-coded. N=9,725 cells. **c** Dot plots showing the expression of CD8+ T cell function relevant genes that are highly expressed in each cluster. The size of the dot corresponds to the percentage of cells expressing the gene in each group and the color represents the average expression level. WT, n=2075 cells; SA, n=2038 cells. **d** Flow cytometry gating strategies in analysis of cellular components of tumor tissues. **e** Flow cytometry analysis of CD69+ and FasL+ GzmB+ cells gated on CD45+CD3+CD8+ T cells in indicated tumor tissues. Data are shown as mean  $\pm$  SEM (n=6 mice for each group). Two-tailed unpaired t-test was performed for the comparisons between groups.

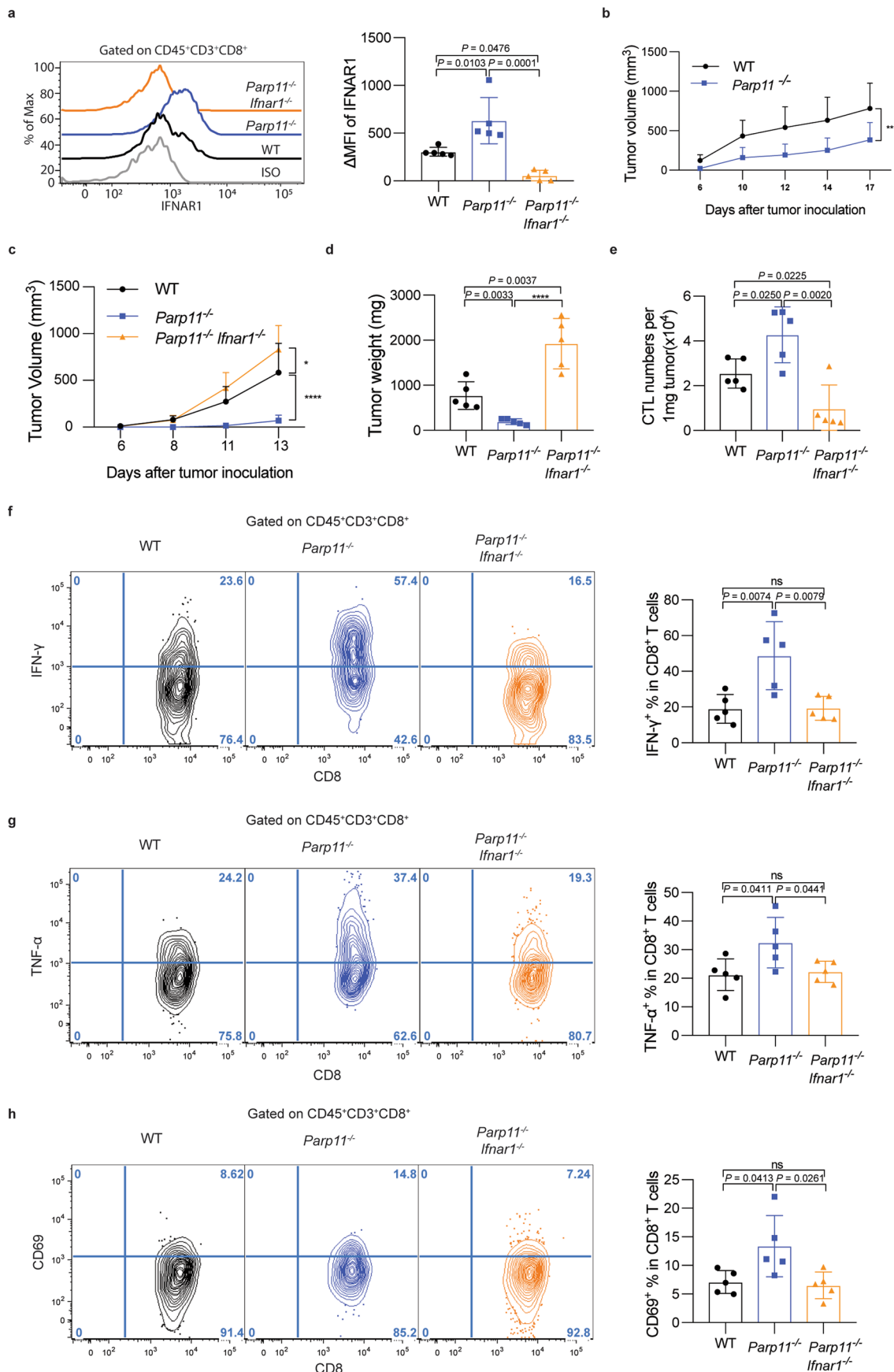


Extended Data Fig. 2 | See next page for caption.

**Extended Data Fig. 2 | Downregulation of CTL IFNAR1 by Treg and adenosine.** **a** WT or SA OT-1 cells were first co-cultured with or without iTregs for 24 h (Treg:OT-1=1:3) and then combined with MC38OVA-luc cells at indicated E:T ratios. Killing of MC38OVA-luc cells was analyzed using luciferase assay as described in Methods. Data are shown as mean  $\pm$  SEM ( $n=3$  co-cultures.) Statistical analysis was performed using two-way ANOVA with Tukey's multiple comparisons test. \* $P=0.0288$ . **b** Tumor associated Tregs were isolated from MC38 WT tumors and cocultured with OT-1 cells for 24 h (Treg: OT-1=1:3). Then analysis of IFNAR1 levels on OT-1 CTL as well as killing of MC38OVA-luc cells (co-cultured at ratio E:T=10:1) was performed as described in Methods. Data are shown as mean  $\pm$  SEM (WT and SA IFNAR1,  $n=3$  co-cultures; WT and SA lysis%,  $n=6$  co-cultures) Statistical analysis was performed using ordinary one-way ANOVA with Tukey's multiple comparisons test. **c** Representative flow cytometry analysis of levels of IFNAR1 on the surface of CD3 $^+$ CD8 $^+$  T cells treated with or without adenosine (Ado, 1mM) prostaglandin E2 (PGE2, 1 $\mu$ g/ml) or tumor growth factor-beta (TGF- $\beta$ , 5ng/ml) for 2 h. **d** Lysis of MC38OVA-luc cells co-cultured in vitro with OT-1 cells pretreated or not with adenosine (Ado, 1mM for 24 h) at indicated E:T ratios. Data are shown as mean  $\pm$  SEM ( $n=3$  co-cultures). Statistical analysis was performed using two-way ANOVA with Tukey's multiple comparisons test. \*\*\* $P < 0.0001$ . **e** Schematic of crosses to generate the *Ifnar1*<sup>ΔCD8</sup> mice. **f** Genotyping analysis of *Ifnar1*<sup>ΔCD8</sup> mice by PCR. **g** Validation of *Ifnar1* ablation in CD8 $^+$  cells using the flow cytometry analysis of IFNAR1 levels on the surface of CD4 $^+$  and CD8 $^+$  T cells in *Ifnar1*<sup>+/+</sup> and *Ifnar1*<sup>ΔCD8</sup> mice. It is representative of  $n=3$  independent experiments.

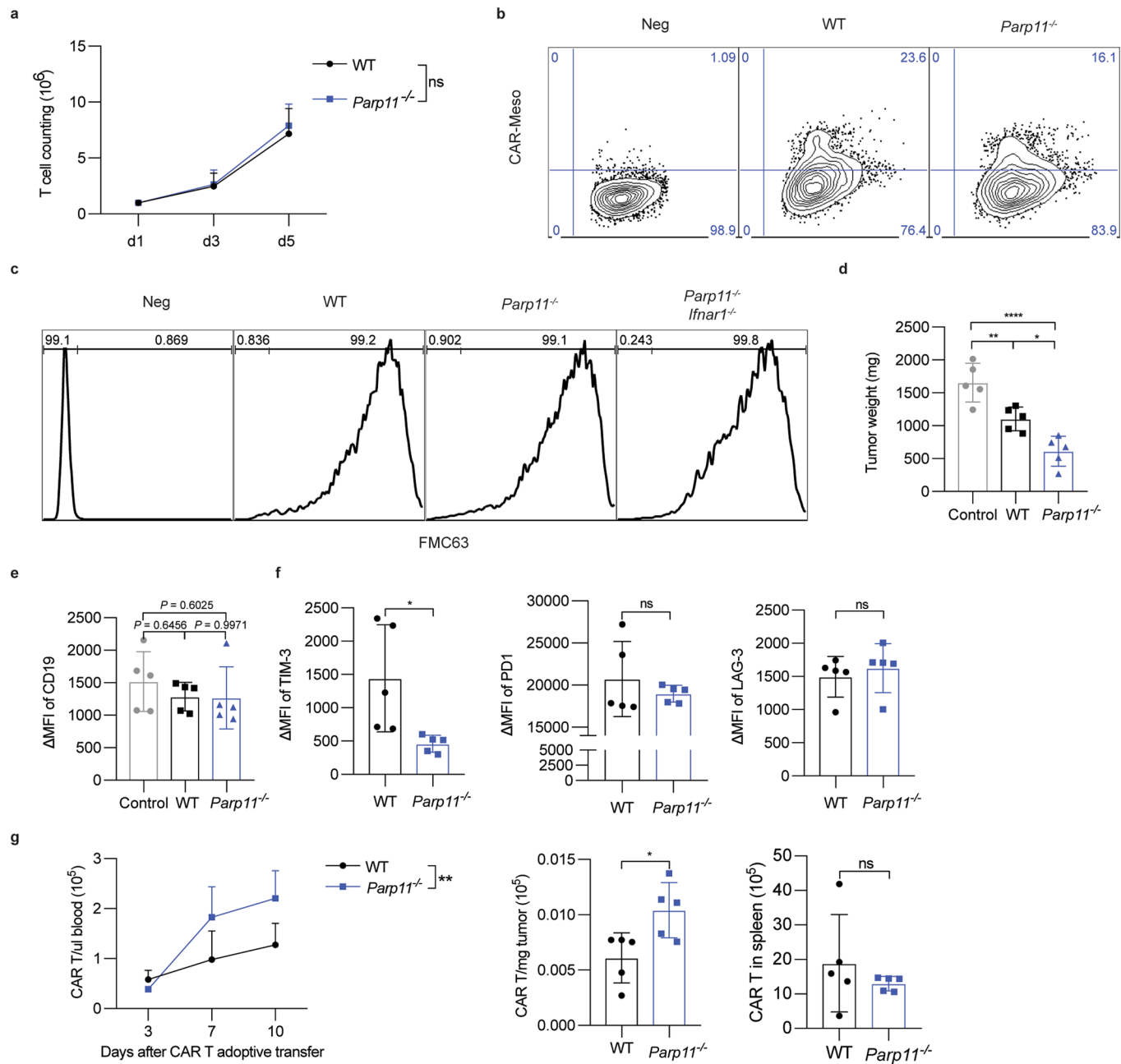


**Extended Data Fig. 3 | PARP11 regulates IFNAR1 downregulation in CD8<sup>+</sup> T cells.** **a** qPCR analysis of mRNA of indicated genes in Jurkat cells treated with adenosine (Ado, 1mM) for 30 min. Data are shown as mean  $\pm$  SEM ( $n=3$  independently treated cell cultures.). Statistical analysis was performed using ordinary one-way ANOVA with Tukey's multiple comparisons test. \*\*\*\*P < 0.0001. **b** Flow cytometry analysis of IFNAR1 levels in EL4 cells, in which indicated genes were knocked out by sgRNA mediated CRISPR-Cas9. Data are shown as mean  $\pm$  SEM.  $n=6$  independently treated cell cultures. Statistical analysis was performed using ordinary one-way ANOVA with Tukey's multiple comparisons test. \*\*\*\*P < 0.0001. **c** Immunoblot and qPCR analysis of efficiency of indicated genes knockout (due to the lack of PARP11-specific antibodies, levels of expression of PARP11 is demonstrated by showing the product of qPCR). Levels of  $\beta$ -actin and  $\beta$ -tubulin are shown as loading controls. **d** ADP-ribosylation of HA- $\beta$ -TrCP immunoprecipitated from 293 T cells treated or not with adenosine (Ado, 1mM, 30 min) as indicated. After treatment, levels of HA- $\beta$ -TrCP in the whole-cell lysate (WCL) was analyzed by immunoblotting. Normalized amounts of lysate containing comparable levels of HA- $\beta$ -TrCP were taken into immunoprecipitation with HA antibody, which was then analyzed by immunoblotting using anti-ADP-ribose antibody and HA antibody. It is representative of 3 independent repeats with similar results. **e** Representative genotyping of *Parp11*<sup>-/-</sup> and *Ifnar1*<sup>-/-</sup> mice. **f** Representative flow cytometry data for Fig. 3g. **h** Representative flow cytometry data for Fig. 3k.

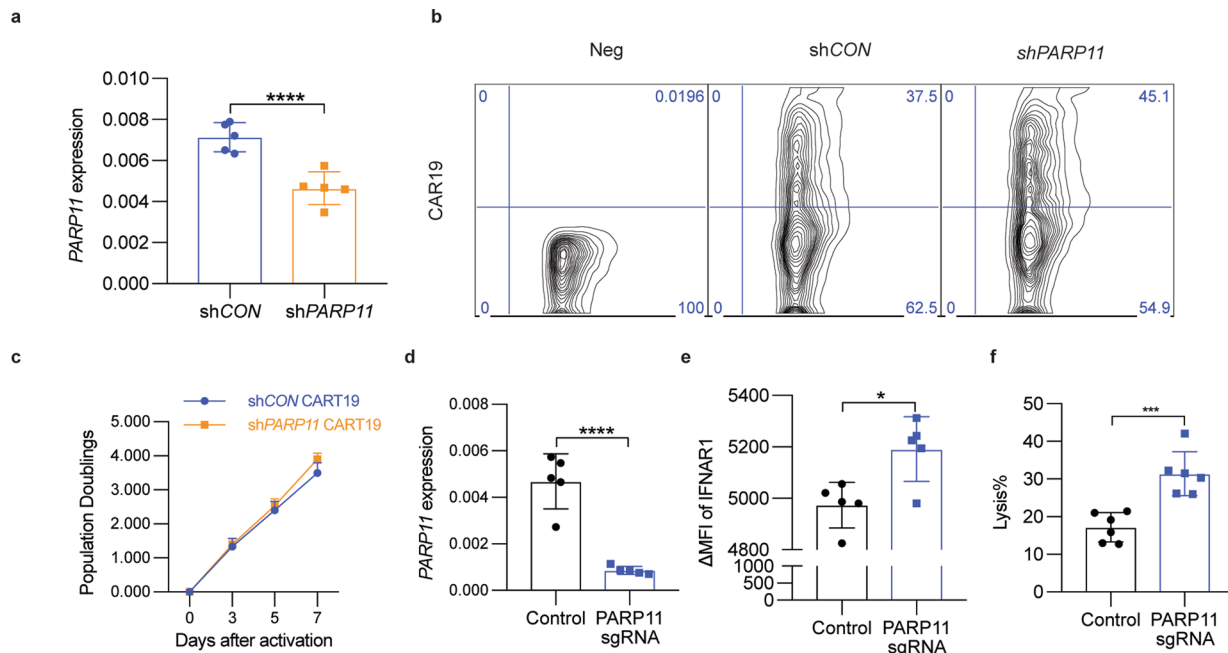


Extended Data Fig. 4 | See next page for caption.

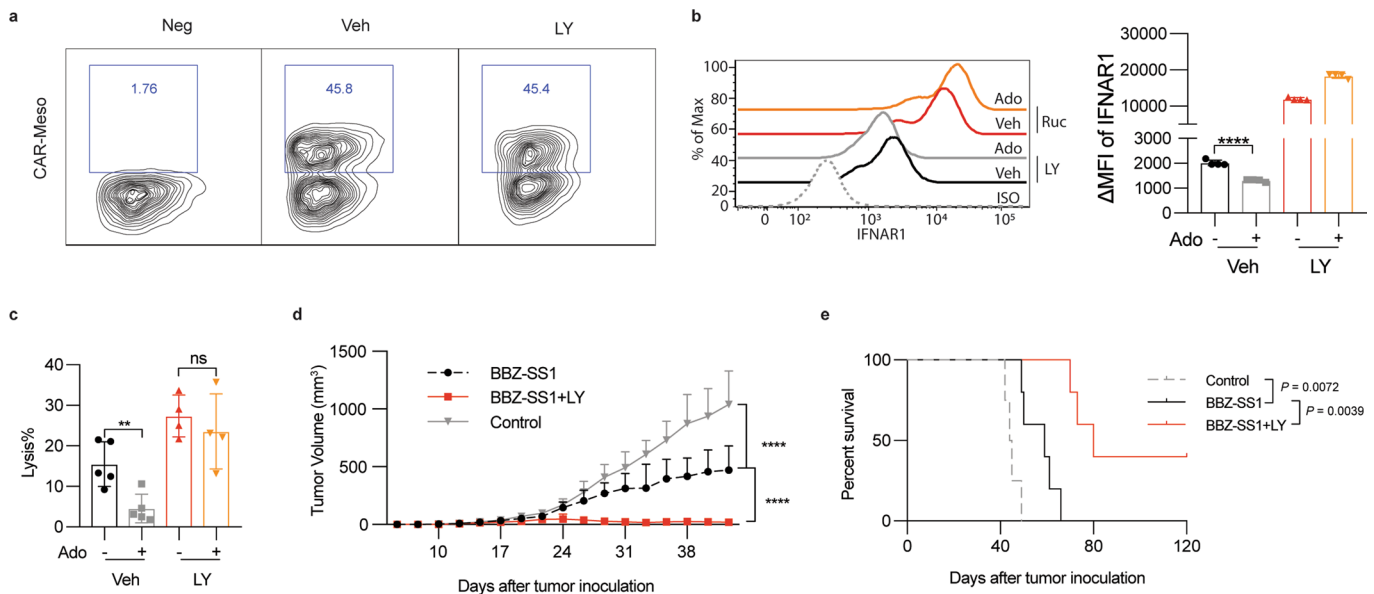
**Extended Data Fig. 4 | Inactivation of intratumoral CTL and robust tumor growth require IFNAR1-dependent function of PARP11 in the TME.** **a** Flow cytometry analysis of levels of IFNAR1 on the surface of CD45<sup>+</sup>CD3<sup>+</sup>CD8<sup>+</sup> T cells in tumor tissues from WT, *Parp11*<sup>-/-</sup> and *Parp11*<sup>-/-</sup>/*Ifnar1*<sup>-/-</sup> mice 13 days after inoculation of s.c. B16F10 tumors ( $0.5 \times 10^5$ / mouse). Statistical analysis was performed using ordinary one-way ANOVA with Tukey's multiple comparisons test. n=5 mice. **b** Growth of s.c. LLC tumors ( $1 \times 10^6$ / mouse) inoculated into WT or *Parp11*<sup>-/-</sup> mice. Statistical analysis was performed using two-way ANOVA with Tukey's multiple comparisons test. \*\*\*P < 0.0001. WT, n=6 mice; *Parp11*<sup>-/-</sup>, n=5 mice. **c** Growth of s.c. B16F10 tumor cells ( $0.5 \times 10^5$ / mouse) inoculated into WT, *Parp11*<sup>-/-</sup>, or *Parp11*<sup>-/-</sup>/*Ifnar1*<sup>-/-</sup> mice. Statistical analysis was performed using two-way ANOVA with Tukey's multiple comparisons test. \*P=0.0387, \*\*\*P < 0.0001. n=5 mice. **d** Quantification of B16F10 tumor weights in mice of indicated genotypes at day 13 after inoculation. Statistical analysis was performed using ordinary one-way ANOVA with Tukey's multiple comparisons test. \*\*\*P < 0.0001. n=5 mice. **e** Flow cytometry analysis of numbers of CD8<sup>+</sup> T cells in B16F10 tumors growing in indicated mice. Statistical analysis was performed using ordinary one-way ANOVA with Tukey's multiple comparisons test. \*\*\*P=0.0007. n=5 mice. **f** Flow cytometry analysis of IFN- $\gamma$ <sup>+</sup> cells gated on CD45<sup>+</sup>CD3<sup>+</sup>CD8<sup>+</sup> T cells in B16F10 tumors growing in indicated mice. Statistical analysis was performed using ordinary one-way ANOVA with Tukey's multiple comparisons test. n=5 mice. **g** Flow cytometry analysis of TNF- $\alpha$ <sup>+</sup> cells gated on CD45<sup>+</sup>CD3<sup>+</sup>CD8<sup>+</sup> T cells in B16F10 tumors growing in indicated mice. Statistical analysis was performed using ordinary one-way ANOVA with Tukey's multiple comparisons test. n=5 mice. **h** Flow cytometry analysis of CD69<sup>+</sup> cells gated on CD45<sup>+</sup>CD3<sup>+</sup>CD8<sup>+</sup> T cells in B16F10 tumors growing in indicated mice. Statistical analysis was performed using ordinary one-way ANOVA with Tukey's multiple comparisons test. n=5 mice.



**Extended Data Fig. 5 | PARP11 undermines tumoricidal activities of CAR T cells.** **a** Proliferation of CD19-BBz CAR T cells prepared from WT or *Parp11*<sup>-/-</sup> mouse splenic T cells. Data are shown as mean  $\pm$  SEM (n=5 samples for each group). Statistical analysis was performed using two-way ANOVA with Tukey's multiple comparisons test. ns, P = 0.6599. **b** Flow cytometry analysis of CAR expression in mouse T cells of indicated genotypes after Meso-BBz transduction. **c** Representative flow cytometry analysis of CAR expression in mouse T cells of indicated genotypes after CD19-BBz transduction. **d** Weight of hCD19-B16F10 s.c. tumors that grew in NSG mice treated with PBS (Control) or adoptively transferred with CD19-BBz CAR T cells (1 $\times$ 10 $6$ /mouse, i.v.) of indicated genotypes as in Fig. 7d. Data are shown as mean  $\pm$  SEM (n=5 mice for each group). Statistical analysis was performed using ordinary one-way ANOVA with Tukey's multiple comparisons test. \*\*P = 0.0087, \*\*\*\*P < 0.0001, \*P = 0.0175. **e** Cell surface expression of human CD19 on the surface of hCD19-B16F10 malignant cells is checked by flow cytometry. Data are shown as mean  $\pm$  SEM (n=5 mice for each group). Statistical analysis was performed using ordinary one-way ANOVA with Tukey's multiple comparisons test. **f** Expression of TIM-3, PD-1 and LAG-3 exhaustion markers by WT or *Parp11*<sup>-/-</sup> CAR T cells isolated from hCD19-B16 subcutaneous tumors from mice described in Extended Data Fig. 5d. Data are shown as mean  $\pm$  SEM (n=5 mice for each group). Statistical analysis was performed using ordinary one-way ANOVA with Tukey's multiple comparisons test. \*\*P = 0.0270. **g** Numbers of WT or *Parp11*<sup>-/-</sup> CAR T cells in the blood, spleen or hCD19-B16 subcutaneous tumors from mice described in Extended Data Fig. 5d. Data are shown as mean  $\pm$  SEM (n=5 mice for each group). Statistical analysis was performed using ordinary one-way ANOVA with Tukey's multiple comparisons test. \*\*P = 0.0038, \*P = 0.0212.



**Extended Data Fig. 6 | Increased efficacy of CAR T cells engineered to inactivate PARP11.** **a** qPCR analysis of PARP11 mRNA in shCON-CD19-BBz or shPARP11-CD19-BBz CAR T cells. Data are shown as mean  $\pm$  SEM ( $n=5$  independently treated cell cultures.). Two-tailed unpaired t-test was performed for the comparisons between groups. \*\*\*\*P < 0.0001. **b** Flow cytometry analysis of CAR expression in human T cells 3 days after shCON-CD19-BBz or shPARP11-CD19-BBz transduction. **c** In vitro proliferation of shCON-CD19-BBz and shPARP11-CD19-BBz CAR T cells following stimulation with anti-CD3/CD28 microbeads. Data are shown as mean  $\pm$  SEM ( $n=3$  independently treated cell cultures). Statistical analysis was performed using two-way ANOVA with Tukey's multiple comparisons test. **d** qPCR analysis of PARP11 mRNA in human WT or PARP11 knockout (PARP11 sgRNA) Meso-BBz CAR T cells. Data are shown as mean  $\pm$  SEM ( $n=5$  independently treated cell cultures). Two-tailed unpaired t-test was performed for the comparisons between groups. \*\*\*\*P < 0.0001. **e** Flow cytometry analysis of IFNAR1 cell surface levels on human WT or PARP11 knockout (PARP11 sgRNA) Meso-BBz CAR T cells. Data are shown as mean  $\pm$  SEM ( $n=5$  independently treated cell cultures). Two-tailed unpaired t-test was performed for the comparisons between groups. \*P = 0.0128. **f** Analysis of killing of EM-Meso-GFP-Luc cells cocultured with human WT or PARP11 knockout (PARP11 sgRNA) Meso-BBz CAR T cells. Data are shown as mean  $\pm$  SEM ( $n=5$  independently treated cell cultures). Two-tailed unpaired t-test was performed for the comparisons between groups. \*\*\*P = 0.0006.



**Extended Data Fig. 7 | Inhibitor of p38 kinase increases the efficacy of CAR T cell therapies.** **a** Representative flow cytometry analysis of CAR expression in human T cells after Meso-BBz transduction and treatment with vehicle or p38 inhibitor Ralimetinib (LY2228820, LY, 5 μM, 72 h). **b** Flow cytometry analysis of levels of IFNAR1 on the surface of Meso-BBz CAR T cells pretreated with indicated inhibitors (LY2228820, LY, 5 μM, 72 h) and then treated by adenosine (Ado, 1mM) for 24 h. Data are shown as mean ± SEM ( $n=4$  independently treated cell cultures). Statistical analysis was performed using ordinary one-way ANOVA with Tukey's multiple comparisons test. \*\*\*\*P < 0.0001. **c** Lysis of EM-Meso-GFP-Luc cells by Meso-BBz CAR T pretreated with inhibitors (LY2228820, LY, 5 μM, 72 h) at indicated conditions (E: T=10:1). Data are shown as mean ± SEM (Veh treated with or without Ado,  $n=5$  co-cultures; LY treated with or without Ado,  $n=5$  co-cultures.). Statistical analysis was performed using ordinary one-way ANOVA with Tukey's multiple comparisons test. \*\*P < 0.0056. **d** Tumor growth of NSG mice that were injected s.c. with  $1 \times 10^6$  EM-Meso-GFP-Luc cells. Mice were i.v. treated with  $2 \times 10^6$  BBZ-SS1 CAR T cells on day 7. BBZ-SS1 CAR T cells were pretreated with LY (5 μM) or Veh for 72 h before injected to mice. Data are shown as mean ± SEM (Control,  $n=7$  mice; BBZ-SS1,  $n=9$  mice; BBZ-SS1 + LY,  $n=10$  mice). Statistical analysis was performed using two-way ANOVA with Tukey's multiple comparisons test. \*\*\*\*P < 0.0001. **e** The Kaplan-Meier analysis of survival of animals from experiment described in Extended Data Fig. 7d ( $n=5$  mice for each group). Statistical analysis was performed using Gehan-Breslow-Wilcoxon test.

## Reporting Summary

Nature Portfolio wishes to improve the reproducibility of the work that we publish. This form provides structure for consistency and transparency in reporting. For further information on Nature Portfolio policies, see our [Editorial Policies](#) and the [Editorial Policy Checklist](#).

### Statistics

For all statistical analyses, confirm that the following items are present in the figure legend, table legend, main text, or Methods section.

n/a Confirmed

- The exact sample size ( $n$ ) for each experimental group/condition, given as a discrete number and unit of measurement
- A statement on whether measurements were taken from distinct samples or whether the same sample was measured repeatedly
- The statistical test(s) used AND whether they are one- or two-sided  
*Only common tests should be described solely by name; describe more complex techniques in the Methods section.*
- A description of all covariates tested
- A description of any assumptions or corrections, such as tests of normality and adjustment for multiple comparisons
- A full description of the statistical parameters including central tendency (e.g. means) or other basic estimates (e.g. regression coefficient) AND variation (e.g. standard deviation) or associated estimates of uncertainty (e.g. confidence intervals)
- For null hypothesis testing, the test statistic (e.g.  $F$ ,  $t$ ,  $r$ ) with confidence intervals, effect sizes, degrees of freedom and  $P$  value noted  
*Give P values as exact values whenever suitable.*
- For Bayesian analysis, information on the choice of priors and Markov chain Monte Carlo settings
- For hierarchical and complex designs, identification of the appropriate level for tests and full reporting of outcomes
- Estimates of effect sizes (e.g. Cohen's  $d$ , Pearson's  $r$ ), indicating how they were calculated

*Our web collection on [statistics for biologists](#) contains articles on many of the points above.*

### Software and code

Policy information about [availability of computer code](#)

Data collection FACS Diva software version 7(BD), Chromium Controller- 10x Genomics.

Data analysis Flowjo V9.9.6 (BD), GraphPad Prism 8 (GraphPad Software Inc.) were used for flow cytometry analysis. RStudio version, R v3.5.3(2019-03-11), Rpckages: Cellranger (<https://support.10xgenomics.com/single-cell-gene-expression/software/overview/welcome>) and Seurat (v3.1.5) were used for scRNASeq analysis. Mouse assembly version mm10 was used for sequence alignments. Strategies for scRNASeq clustering, cell projection, differential gene expression are similar to previously described (see methods), and script are available upon request.

For manuscripts utilizing custom algorithms or software that are central to the research but not yet described in published literature, software must be made available to editors and reviewers. We strongly encourage code deposition in a community repository (e.g. GitHub). See the Nature Portfolio [guidelines for submitting code & software](#) for further information.

### Data

Policy information about [availability of data](#)

All manuscripts must include a [data availability statement](#). This statement should provide the following information, where applicable:

- Accession codes, unique identifiers, or web links for publicly available datasets
- A description of any restrictions on data availability
- For clinical datasets or third party data, please ensure that the statement adheres to our [policy](#)

Mouse scRNASeq data are all available on GEO (accession number: GSE171055).

# Field-specific reporting

Please select the one below that is the best fit for your research. If you are not sure, read the appropriate sections before making your selection.

Life sciences

Behavioural & social sciences

Ecological, evolutionary & environmental sciences

For a reference copy of the document with all sections, see [nature.com/documents/nr-reporting-summary-flat.pdf](https://nature.com/documents/nr-reporting-summary-flat.pdf)

## Life sciences study design

All studies must disclose on these points even when the disclosure is negative.

|                 |  |
|-----------------|--|
| Sample size     | No statistical methods were used to pre-determine sample size. Sample sizes were estimated based on preliminary experiments, with an effort to achieve a minimum of n=3, mostly n=5 mice per treatment group, which proved sufficient to determine reproducible results. |
| Data exclusions | For Seurat analysis, we excluded cells with low and high number of detected transcripts.   |
| Replication     | All experiments were reliably reproduce. All experiments (except for scRNAseq) were performed independently at least two times. scRNAseq samples were pooled from 3 mice in each group.  |
| Randomization   | Mice with matched sex and age are randomized into different treatment groups.  |
| Blinding        | Quantification of mouse tumor sizes, immune cell infiltration and function analysis were blinded by de-identifying samples. Investigators were blinded to group allocation during data collection.   |

## Reporting for specific materials, systems and methods

We require information from authors about some types of materials, experimental systems and methods used in many studies. Here, indicate whether each material, system or method listed is relevant to your study. If you are not sure if a list item applies to your research, read the appropriate section before selecting a response.

| Materials & experimental systems    |   | Methods                             |  |
|-------------------------------------|---|-------------------------------------|--|
| n/a                                 | Involved in the study   | n/a                                 | Involved in the study                              |
| <input type="checkbox"/>            | <input checked="" type="checkbox"/> Antibodies                  | <input type="checkbox"/>            | <input checked="" type="checkbox"/> ChIP-seq       |
| <input type="checkbox"/>            | <input checked="" type="checkbox"/> Eukaryotic cell lines       | <input type="checkbox"/>            | <input checked="" type="checkbox"/> Flow cytometry |
| <input checked="" type="checkbox"/> | <input type="checkbox"/> Palaeontology and archaeology          | <input checked="" type="checkbox"/> | <input type="checkbox"/> MRI-based neuroimaging    |
| <input type="checkbox"/>            | <input checked="" type="checkbox"/> Animals and other organisms |                                     |  |
| <input type="checkbox"/>            | <input checked="" type="checkbox"/> Human research participants |                                     |  |
| <input checked="" type="checkbox"/> | <input type="checkbox"/> Clinical data                          |                                     |  |
| <input checked="" type="checkbox"/> | <input type="checkbox"/> Dual use research of concern           |                                     |  |

## Antibodies

### Antibodies used

The following antibodies were used for flow cytometry:

Purified anti-mouse CD16/32 antibody Biolegend 101301 clone: 93 dilution: 50x  
 FITC anti-mouse CD45 Antibody Biolegend 103108 clone: 30-F11 dilution: 200x  
 APY CY7 anti-mouse CD8 Antibody Biolegend 126619 clone: YTS156.7.7 dilution: 200x  
 PE/CY7 anti-mouse CD8 Antibody Biolegend 100721 clone: 53-6.7 dilution: 200x  
 Viability dye Invitrogen 65-0866-14 dilution: 1000x  
 PE anti-mouse CD8 Antibody Invitrogen 12-0081-81 clone: 53-6.7 dilution: 200x  
 PE/CY7 anti-mouse CD8 Antibody Biolegend 100721 clone: 53-6.7 dilution: 200x  
 FITC anti-mouse CD8 Antibody Biolegend 100705 clone: 53-6.7 dilution: 200x  
 BV605 anti-mouse CD3 Antibody Biolegend 100237 clone: 17A2 dilution: 200x  
 PE-Cyanine 5.5 anti-mouse CD4 Antibody Invitrogen 35-0042-80 clone: RM4-5 dilution: 200x  
 AF700 anti-mouse GzmB Antibody Biolegend 372221 clone: QA16A02 dilution: 200x  
 PE anti-mouse TNF- $\alpha$  Antibody Biolegend 506305 clone: MP6-XT22 dilution: 200x  
 PE/Cy7 anti-mouse IFN- $\gamma$  Antibody Biolegend 505825 clone: XMG1.2 dilution: 200x  
 FITC anti-mouse CD4 Antibody Biolegend 100405 clone: GK1.5 dilution: 200x  
 PE anti-mouse IFNAR-1 Antibody Biolegend 127311 clone: MAR1-5A3 dilution: 200x  
 PE anti-mouse CD178 (Fasl) Antibody Biolegend 106605 clone: MFL3 dilution: 200x  
 APC/Cy7 anti-mouse CD8b Antibody Biolegend 126619 clone: YTS156.7.7 dilution: 200x  
 Brilliant Violet 510™ anti-mouse TNF- $\alpha$  Antibody Biolegend 506339 clone: MP6-TP22 dilution: 200x  
 Brilliant Violet 510™ anti-mouse CD3 Antibody Biolegend 100233 clone: 17A2 dilution: 200x  
 PE anti-mouse FOXP3 Antibody Biolegend 126403 clone: MF-14 dilution: 200x  
 PE/Cy5 anti-mouse CD8a Antibody Biolegend 100709 clone: 53-6.7 dilution: 200x

PerCP anti-mouse CD8a Antibody Biolegend 100731 clone: 53-6.7 dilution: 200x  
 PE/Cy7 anti-mouse CD3 Antibody Biolegend 100219 clone: 17-A2 dilution: 200x  
 Phospho-CREB (Ser133) (87G3) Rabbit mAb (PE Conjugate) cst 14228 clone: 87G3 dilution: 200x  
 PKA C- $\alpha$  Antibody cst 4782 dilution: 200x

The following antibodies were used for IP and Western Blot analysis.  
 Recombinant Anti-p38 (phospho T180) antibody [EPR16587] Abcam Ab178867 dilution: 1000x  
 $\beta$ -Tubulin Antibody CST 2146S dilution: 5000x  
 p38 $\alpha$  Antibody (N-20) santa cruz biotechnology sc-728 dilution: 1000x  
 $\beta$ -TrCP (D13F10) Rabbit mAb CST 4394 dilution: 1000x  
 Mono- and polyubiquitinylated conjugates monoclonal antibody (FK2) Enzo Life Sciences BML-PW8810-0100 dilution: 1000x  
 Recombinant Anti-Interferon alpha/beta receptor 1 antibody [EP899Y] Abcam Ab45172 dilution: 1000x  
 GAPDH (D16H11) XP<sup>®</sup> Rabbit mAb CST 5174 dilution: 5000x  
 Anti-mono- and poly-ADP-ribose binding reagent Millipore MABE1075 dilution: 1000x  
 Myc-Tag mAb Abmart M20002H dilution: 1000x  
 Anti-HA tag antibody Abcam ab9110 dilution: 1000x  
 Anti-Flag antibody Sigma F7425 dilution: 1000x  
 Streptavidin-HRP CST 3999 dilution: 1000x

#### Validation

All the antibodies are validated for the use of immunofluorescence, IP, and western blot analyses. Data are available on the manufacturer's website. The antibodies have been validated by the manufacturer and, or in this paper.

## Eukaryotic cell lines

#### Policy information about [cell lines](#)

##### Cell line source(s)

Mouse cell lines MC38, B16F10, LLC and EL4 and human Jurkat, NALM6 and 293T cells were purchased from ATCC and maintained according to ATCC recommendations. Mouse B16F10 cells bearing human CD19 (hCD19-B16F10) were generated by transduction and subsequent selection. Mouse MC38OVA and human EM-Meso-GFP-Luc cell line were generously provided by Dr. Susan Ostrand-Rosenberg (University of Maryland, Baltimore, USA) and by Dr. Edmund Moon (University of Pennsylvania, Philadelphia, USA), respectively. MC38OVA and hCD19-B16F10 cells were further engineered to stably express Firefly luciferase.

##### Authentication

MC38, B16F10-hCD19, EM-Meso-GFP-Luc cells were injected s.c. into mice and tumor volume was followed. No other authentication was performed.

##### Mycoplasma contamination

All cell lines tested negative for mycoplasma.

##### Commonly misidentified lines (See [ICLAC](#) register)

No commonly misidentified cell lines were used in the study.

## Animals and other organisms

#### Policy information about [studies involving animals; ARRIVE guidelines](#) recommended for reporting animal research

##### Laboratory animals

All mice had water ad libitum and were fed regular chow. Mice were maintained in a specific-pathogen-free facility in accordance with American Association for Laboratory Animal Science guidelines. C57BL/6 littermate Ifnar1+/+ ('WT') and Ifnar1S526A mice (SA) were described previously; the SA mice were donated to Jackson Labs and are available from this source (C57BL/6-Ifnar1tm1.1Syfu/J; stock No. 035564). As described previously, Parp11 knockout mice exhibited teratozoospermia and male infertility but otherwise developed normally and did not display any overt pathology.

Ifnar1 $^{-/-}$  mice (B6(Cg)-Ifnar1tm1.2Ees/J; stock No. 028288), Ifnar1f/f mice (B6(Cg)-Ifnar1tm1.1Ees/J, stock No. 028256), C57BL/6-Tg(Cd8a-cre)1Itan/J (CD8-cre, stock No. 008766) and NOD.Cg-Prkdcscid Il2rgtm1Wjl/SzJ (NSG, stock No. 005557) mice were purchased from Jackson Laboratory. CD8-cre mice were crossed with Ifnar1f/f mice to generate CD8-cre::Ifnar1f/f mice and CD8-cre::Ifnar1f/f litter-mates.

Mice used in the experiments are sex mixed and 6-10 wks age matched.

##### Wild animals

The study did not involve wild animals.

##### Field-collected samples

The study did not involve field-collected samples.

##### Ethics oversight

All animal experiments were approved by the Institutional Animal Care and Use Committee of the University of Pennsylvania and were carried out in accordance with the IACUC guidelines.

Note that full information on the approval of the study protocol must also be provided in the manuscript.

## Human research participants

#### Policy information about [studies involving human research participants](#)

##### Population characteristics

Not involved.

##### Recruitment

Not involved.

Ethics oversight

Not involved.

Note that full information on the approval of the study protocol must also be provided in the manuscript.

## Flow Cytometry

### Plots

Confirm that:

- The axis labels state the marker and fluorochrome used (e.g. CD4-FITC).
- The axis scales are clearly visible. Include numbers along axes only for bottom left plot of group (a 'group' is an analysis of identical markers).
- All plots are contour plots with outliers or pseudocolor plots.
- A numerical value for number of cells or percentage (with statistics) is provided.

### Methodology

#### Sample preparation

Tumors or spleens were collected and incubated in dissociation solution with 2mg/ml Collagenase II (MP Biomedicals), or 1 mg/ml Collagenase IV (Roche) plus 100 µg/ml DNase I (Roche) for 1 h with continuous agitation. Cells were filtered by 70µm cell strainer and resuspended with FACS buffer (PBS with 1% BSA, 1mM EDTA).

#### Instrument

BD LSRFortessa

#### Software

FACS Diva software version 7 (BD)

#### Cell population abundance

Purity of cell population checked by flow cytometry.

#### Gating strategy

Gating for immune cells in tumor tissues: 1. Gate on FSC-A vs. SSC-A was set to include all cell populations. 2. Gate on FSC-A vs. FSC-H to exclude doublets. 3. Gate on FSC-A vs. Viability to exclude dead cells. 4. Gate on CD45+ vs. CD3+. 5. Gate on CD4+ or CD8+. 6. Further analyze protein levels in different cell subsets.

- Tick this box to confirm that a figure exemplifying the gating strategy is provided in the Supplementary Information.